Behaviour of steel-fibre-reinforced concrete beams under high-rate loading

Pegah Behinaein [1a], Demetrios M. Cotsovos[1b] and Ali A. Abbas[*2]

[1]Institute of Infrastructure and Environment, School of the Built Environment, Heriot-Watt University, Edinburgh EH14 4AS, UK

[2]School of Architecture, Computing and Engineering, University of East London, London E16 2RD, UK

Abstract. The present study focuses on examining the structural behaviour of steel-fibre-reinforced concrete (SFRC) beams under high rates of loading largely associated with impact problems. Fibres are added to the concrete mix to enhance ductility and energy absorption, which is important for impact-resistant design. A simple, yet practical non-linear finite-element analysis (NLFEA) model was used in the present study. Experimental static and impact tests were also carried out on beams spanning 1.3 meter with weights dropped from heights of 1.5 m and 2.5 m, respectively. The numerical model realistically describes the fully-brittle tensile behaviour of plain concrete as well as the contribution of steel fibres to the post-cracking response (the latter was allowed for by conveniently adjusting the constitutive relations for plain concrete, mainly in uniaxial tension). Suitable material relations (describing compression, tension and shear) were selected for SFRC and incorporated into ABAQUS software Brittle Cracking concrete model. A more complex model (i.e. the Damaged Plasticity concrete model in ABAQUS) was also considered and it was found that the seemingly simple (but fundamental) Brittle Cracking model yielded reliable results. Published data obtained from drop-weight experimental tests on RC and SFRC beams indicates that there is an increase in the maximum load recorded (compared to the corresponding static one) and a reduction in the portion of the beam span reacting to the impact load. However, there is considerable scatter and the specimens were often tested to complete destruction and thus yielding post-failure characteristics of little design value and making it difficult to pinpoint the actual load-carrying capacity and identify the associated true ultimate limit state (ULS). To address this, dynamic NLFEA was employed and the impact load applied was reduced gradually and applied in pulses to pinpoint the actual failure point. Different case studies were considered covering impact loading responses at both the material and structural levels as well as comparisons between RC and SFRC specimens. Steel fibres were found to increase the load-carrying capacity and deformability by offering better control over the cracking process concrete undergoes and allowing the impact energy to be absorbed more effectively compared to conventional RC members. This is useful for impact-resistant design of SFRC beams.

[*]Corresponding author, Senior Lecturer, PhD, E-mail: abbas@uel.ac.uk
[a] Ph.D. Student, BSc, MSc, E-mail: pb2@hw.ac.uk
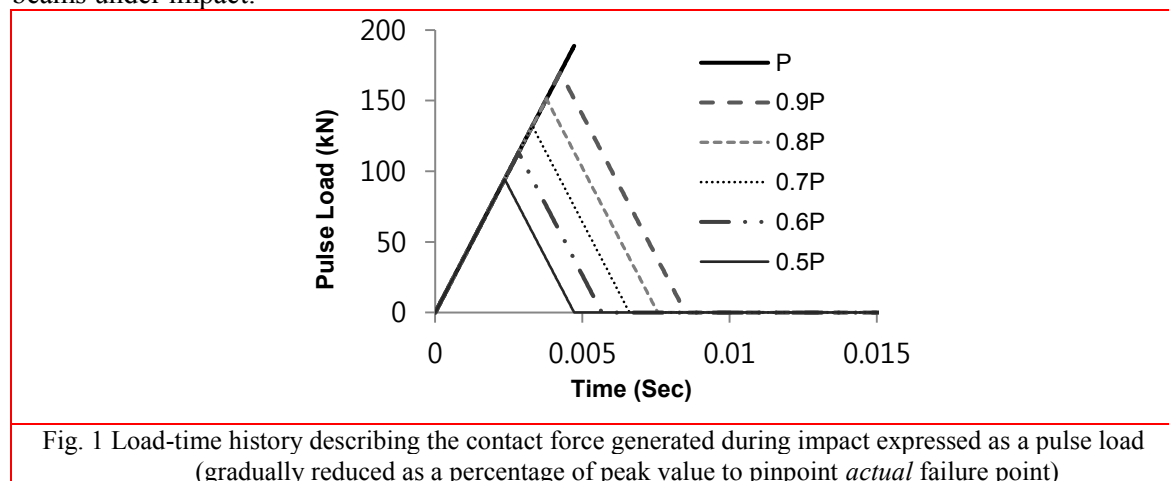[b] Associate Professor, Ph.D., E-mail: d.cotsovos@hw.ac.uk

1. Introduction

Modern infrastructure faces increasing demands for a variety of activities and services such as affordable housing, faster transportation and higher energy production. This has led to the development of complex structural systems such as high-rise buildings, bridges, tunnels, slab-track for high-speed trains, off-shore and marine structures, nuclear power plants and storage and industrial facilities. Such structures are fully or partially constructed from reinforced concrete (RC) and are often required to meet significant resilience demands – which are bound to increase as a result of climate change – in order to safely withstand loads imposed at higher rates and intensities than those considered in current design codes. This has prompted the development of new advanced construction materials, with enhanced material properties compared to those of plain concrete, such as steel fibres, to meet such demands.

It has been established numerically (Cotsovos *et al.*, 2008, Cotsovos, 2010, Saatci and Vecchio, 2009, Kishi *et al.*, 2011) and experimentally (Abbas *et al.*, 2010, May *et al.*, 2006) that the dynamic structural responses of RC members differ to those observed under corresponding static loading once certain thresholds of applied loading rate are surpassed. The observed shift in structural response with increasing loading rates is considered to be associated with (a) structural arrangements (such as geometry, reinforcement and boundary details), (b) the brittle nature and tri-axiality characterising concrete material behaviour, (c) the nature of the problem at hand (i.e. a wave propagation problem within a highly non-linear material) and (d) the development of high strain rates within concrete and steel which is widely considered to affect material behaviour, i.e. strain-rate sensitivity (Cotsovos and Pavlović, 2012). The current work aims to examine the potential benefits of introducing steel fibres to the concrete mix in order to enhance the responses of (the otherwise RC) structural elements under high rate loading due to impact. The work is based on dynamic Non-linear Finite Element Analysis (NLFEA), which was initially validated using existing experimental data to ascertain its accuracy before the subsequent parametric studies were carried out. The work builds on previous NLFEA-based studies on various steel-fibre-reinforced concrete (SFRC) structural configurations subjected to both static monotonic and cyclic loading. The specimens covered a wide practical range from simply-supported beams to more complex structural systems characterised by a certain degree of static indeterminacy, such as continuous columns and beam-column sub-assemblages (Abbas *et al.*, 2016, 2014a,b,c,d). Both previous and current studies utilise a material model for SFRC that is focused on realistically describing the fully-brittle tensile behaviour of plain concrete as well as the contribution of steel fibres to the post-cracking response. The constitutive relations were incorporated into ABAQUS (2016) software Brittle Cracking concrete model in order to allow for the effects of fibres. Comparative studies between numerical predictions and experimental results demonstrated that, despite the simplicity of the model, it provided realistic predictions concerning the structural responses up to failure for the different SFRC configurations studied. The previous work (particularly under seismic loading) is extended herein in order to realistically describe the response – up to failure – of SFRC structural simply-supported beams under high-rate (i.e. impact) loading. In addition to the brittle cracking model, the more advanced "damage plasticity" model (also available in ABAQUS) is also employed in the present study for purpose of comparison. Once validated against available test data, the numerical predictions obtained are used to study the mechanics underlying the behaviour of RC and SFRC beam specimens when subjected to impact loading as well as the effects of steel fibres on the ensuing structural responses.

Published data (Cotsovos *et al.*, 2008, Cotsovos, 2010, Saatci and Vecchio, 2009, Kishi *et al.*, 2011,

Abbas *et al.*, 2010, May *et al.*, 2006, Cotsovos and Pavlović, 2012) obtained from drop-weight experimental tests on RC beams (i.e. without fibres) indicates that the response under impact loading differs significantly from that established during equivalent static testing, resulting in an increase of the maximum sustained load and a reduction in the portion of the beam span reacting to the impact load. However, there is considerable scatter making it difficult to ascertain the effect of loading rate on various aspects of RC and SFRC structural responses. Crucially, most of the available test data obtained from drop-weight tests conducted on RC and SFRC beam specimens is associated with a *post*-impact specimen physical state often characterised by significant concrete disintegration and low values of residual stiffness and load-carrying capacity.   To address this, a dynamic NLFEA-based parametric study was carried out to assess (i) the true ultimate limit state (ULS) and associated load-carrying capacity exhibited by the specimens when subjected to different loading rates and (ii) the effect of steel fibres on exhibited structural response. The form of the imposed impact load was described by a simplified force-time function which consists of an ascending and a subsequent descending branch, in which the rate of loading (associated with the ascending branch) is assumed equal to the rate of unloading (of the descending branch). The impact load was reduced gradually and applied in pulses to pinpoint the actual failure point (see Fig. 1). Therefore, during the parametric studies, each beam specimen was subjected to a series of pulse loads characterised by different loading rates and intensities in order to identify the true load carrying capacity of the specimens. Different case studies were considered (and initially validated against experimental data), covering impact loading responses at both the material and structural levels as well as comparisons between RC and SFRC specimens. Key aspects of structural behaviour such as maximum sustained load, load-deflection curves, deformation profiles and cracking patterns under different rates and intensities of impact loading were examined. The ultimate aim is to form the basis of a new practical assessment and design method for SFRC beams under impact.

Fig. 1 Load-time history describing the contact force generated during impact expressed as a pulse load (gradually reduced as a percentage of peak value to pinpoint *actual* failure point)

The history of fibre-reinforced materials started in ancient Egypt over 2000 years ago with mud bricks reinforced with straw fibres. In more recent times, alternative fibres were introduced in the 1960s, such as steel, glass, and synthetic fibres such as polypropylene fibres etc. Early investigation into the application of SFRC was carried out by Romualdi and Batson (1963) resulted in its application in the pavement construction. Since then, fibres have become widely adopted in different structural applications, for instance in concrete pipes, pavement slabs and

more recently, it has been used in suspended slabs (Destrée, 2001). The introduction of steel fibres into the concrete mix can also lead to a reduction of transverse (i.e. shear) reinforcement such as beams, walls, joint regions (Abbas *et al.*, 2016, 2014a,b,c,d, Nadine, 2011) without compromising design codes (Eurocode 2, 2004, Eurocode 8, 2004) performance requirements for strength and ductility. The main benefit of such reduction is to alleviate reinforcement congestion due to dense arrangement and spacing of shear links in the critical regions of RC structures, as dictated in design codes such as the Eurocode 8 (2004) for seismic-resistant design in order to avoid brittle failure modes. The present research work focuses on the behaviour of steel fibres and other fibre types are outside the scope of the study.

2. Background of SFRC impact tests

Several experimental studies have been carried on SFRC specimens under impact loading (Naaman and Gopalaratnam, 1983, Xu *et al.*, 2012, Zhang *et al.*, 2014). The majority of these studies employ drop weight testing, in which a steel striker is allowed to fall from a pre-defined height onto a specific (usually the mid-span) region of the structural element considered such as beams and slabs. A number of SFRC specimens have been tested to date under impact loading in order to assess the effect of various parameters associated with the fibres used (such as shape, aspect ratio, volume fraction) on the observed behaviour. The test data collected reveals that the addition of fibres can enhance the maximum sustained load, ductility, toughness and crack control in SFRC members under impact loading compared to their corresponding conventionally-reinforced concrete members (Xu *et al.*, 2012). However, it should be noted that the experimental data is characterised by considerable scatter, which predominantly reflects the difficulty in correlating the measured response to the actual physical state of the specimens. In fact, the measured maximum value of the contact force generated (usually referred to as the maximum sustained load) frequently corresponds to a *post*-impact specimen with a physical state characterised by significant concrete disintegration as well as low residual load-bearing capacity and stiffness (Cotsovos, 2010, Cotsovos and Pavlović, 2012). This stage of structural response has little practical significance as it depends heavily on *post*-failure mechanisms for transferring the applied loads to the specimen supports. In view of the above, the available test data cannot provide detailed insight into the mechanisms underlying structural response, but only a *qualitative* description of the effect of the loading rate and the use of steel fibres on specimen behaviour.

3. Investigating the behaviour of SFRC beams using NLFEA

NLFEA is often used for investigating a wider range of concrete problems (Kotsovos and Pavlović, 1995, Kotsovos et al. 2008) in a safer and more cost-effective manner compared to drop-weight testing as well as providing detailed insight into the mechanisms underlying SFRC structural responses under high-rate loading, which cannot be achieved solely on the basis of the available test data. The present work employs a well-known commercial finite element analysis (FEA) software ABAQUS (2016), which can carry out 3D static and dynamic NLFEA. It incorporates both, a simple brittle model, termed "Brittle Cracking model", and a more complex "Damaged Plasticity model" in order to describe concrete material behaviour.

3.1 Modellling of concrete material behaviour

The Brittle Cracking (BC) model is purpose-built for materials the behaviour of which is dominated by tensile cracking (ABAQUS, 2016). This is largely true in the case of RC flexural structural elements where cracks form due to the development of tensile strains within the concrete medium. Such cracks gradually extend with increasing levels of applied loading, ultimately leading to structural failure and collapse. This is particularly useful for the present study on SFRC performance as it allows for modelling the effect of steel fibres on the concrete behaviour in tension, especially after the *onset* of cracking. It is interesting to note that in the "Brittle Cracking model", the behaviour of concrete in compression is modelled as being linear elastic in order to enhance the numerical stability of the solution process. By adopting this simplification, emphasis is focused on realistically describing the all-important tensile response. Furthermore, as the present NLFEA is carried out using 3D modelling, at least one principal stress is required to be tensile to trigger cracking (this is the salient feature of concrete behaviour which is predominantly brittle) and this is well captured by the Brittle Cracking model. So, although the model assumes elastic behaviour in compression for efficiency purposes, this does not affect the accuracy as the predictions are in good agreement with experimental data (as discussed in the present study). This basic yet profound and focused approach allows one to develop a more fundamental understanding of aspects affecting the structural response of SFRC.

The development of the Damage Plasticity (DP) model is based on the Drucker–Prager strength hypothesis (ABAQUS, 2016). Concrete material behaviour in compression and tension is described separately through the use of non-linear stress-strain curves with post-peak branches (which are softening in compression and can be softening or hardening in tension). A scalar-damage model is employed to account for the reduction of stiffness occurring due to degradation resulting from tensile cracking or crushing (ABAQUS, 2016). Degradation is assumed isotropic and dependent on a single parameter (i.e. scalar stiffness degradation variable), the value of which ranges from 0 for an undamaged state to 1 for a fully damaged state. The model also contains parameters such as the

initial undamaged and the degraded elastic stiffness of concrete as well as the equivalent plastic strains in tension or compression (which is associated with the micro-cracking and the crushing processes that concrete is considered to undergo). These parameters essentially control the evolution of the yield surface and the degradation of the elastic stiffness. When unloading occurs after entering the strain softening (i.e. descending) branch of the stress-strain curves, the degradation becomes more pronounced as the plastic strain increases. Important parameters that need to be defined in the DP model are (i) the dilation angle ψ (i.e. the angle of inclination of the failure surface in relation to the hydrostatic axis) which controls the plastic flow and (ii) the viscosity parameter (ABAQUS, 2016).

3.2 Modelling of the contribution of steel fibres to concrete behaviour

The introduction of fibres into the concrete mix can enhance both the concrete *material* behaviour (predominantly in tension) and RC *structural* response. More specifically fibres contribute ductile characteristics to an otherwise brittle plain concrete material (by offering better control over the cracking process concrete undergoes) resulting in an increase in its capacity to absorb energy (Abbas *et al.*, 2016, 2014a,b,c,d). The latter is of significance to structures under impact loads. To date, many experimental investigations have been conducted in order to study

the effect of fibres on structural concrete *material* behaviour (Zhang *et al.*, 2014, Trottier and Banthia, 1994, Robins *et al.*, 2002, RILEM, 2003). The vast majority of these tests have been carried out on prisms and cylinders subjected to compression, direct and indirect tension and flexure. Such studies aim at assessing the effect of fibres on:

- important aspects of concrete material behaviour such as compressive strength f_c, tensile strength f_t, the elasticity modulus E_c, and the stress-strain curve under uniaxial compression or tension after cracking, and
- the cracking process that fibrous concrete undergoes, which is dependent on the fibre content, the bond strength and pull out behaviour of fibres bridging a crack as the crack becomes wider with increasing levels of applied loading.

The performance of SFRC is influenced by a number of parameters associated with the fibres such as shape, length, aspect ratio, and volume fraction and the concrete mix (Zhang *et al.*, 2014, Trottier and Banthia, 1994, Robins *et al.*, 2002, RILEM, 2003). The effect of fibres on concrete material behaviour in tension can be mainly observed after the onset of cracking as they induce ductile characteristics to the post cracking behaviour of SFRC compared to the fully brittle behaviour exhibited by plain concrete (Kotsovos and Pavlović, 1995, Zisopoulos *et al.*, 2000, Kotsovos, 2015). Depending on the type and amount of fibres used, the post cracking behaviour may be described as strain-softening or strain-hardening. The residual strength of SFRC is the result of steel fibres bridging the cracks and the bond between the fibre and the surrounding concrete. The addition of steel fibres at small dosages to the concrete mix results in a softening post-cracking response, whilst the provision of higher fibre contents leads to a hardening behaviour as the fibres undertake the tensile forces which are acting normal to the plane of crack and will cause the increase in *residual* tensile strength (the tensile strength of concrete itself is unaffected as fibres act only after *onset* of cracking by bridging the cracks). In the latter hardening-response case, failure eventually occurs to pull-out of the fibres and the development of finer and more distributed multiple cracks as opposed to the single crack associated with softening behaviour. In the present study, the material constitutive model proposed by Lok and Xiao (1999) was adopted in order to define the post-cracking tensile stress-strain relationship for SFRC. Several other models were considered in previous studies by the authors (Abbas *et al.*, 2016, 2014a,b,c,d) and it was found that this is most suitable model as it allowed for different fibre aspect ratios and bond characteristics.

3.3 Non-linear solution strategy

During each time step the equation of motion governing the non-linear dynamic impact problem considered is solved as a sequence of equivalent static problems through the use of the Newmark family of approximation methods (Abbas *et al.*, 2014d, Zisopoulos *et al.*, 2000, Kotsovos, 2015). At the beginning of each iteration and based on the values of displacement, velocity and acceleration obtained from the previous iteration, the effective stiffness and load matrix are calculated and an equivalent static problem is formulated (Kotsovos, 2015). The equivalent static problem is solved through an iterative procedure based on a modified Newton-Raphson method (Kotsovos and Pavlović, 1995, Kotsovos, 2015, Zienkiewicz and Taylor, 2005). During the solution process of the equivalent static problem, every Gauss point is checked to determine whether loading or *un*loading takes place and to establish whether any new cracks form or older ones close. Depending on the results of the previous checks, changes are introduced to the stress-strain matrices of the individual FE's and to the stiffness matrix of the structure.

Convergence is checked locally at each Gauss point, this involves the use of the constitutive relations for the calculation of the stresses increments which correspond to the estimated values of the strain increments. Once the values of the strain and the corresponding stress increments become less than a small predefined value (i.e. convergence criterion) then convergence is accomplished. When this is not achieved, the residual forces are calculated and are then re-imposed onto the FE model of the RC form investigated until convergence is finally achieved.

3.4 Modelling of cracking

The cracking process that concrete undergoes is modelled through the use of the smeared crack approach (Kotsovos and Pavlović, 1995, Kotsovos, 2015, Zienkiewicz and Taylor, 2005). A crack is considered to form when the predicted stress in a given part of the structure corresponds to a point in the principal stress space that lies outside the surface defining the failure criterion for concrete, thus resulting in localised failure of the material. The plane of the crack is assumed normal to the direction in which the smallest principal stress acts (smallest compressive or largest tensile stress). A simple Rankine failure criterion is used to detect crack initiation (i.e. a crack forms when the maximum principal tensile stress exceeds the specified tensile strength of concrete). Constitutive calculations are performed independently at each integration point of the finite element model. The presence of cracks enters into these calculations by the way in which the cracks affect the stress and material stiffness associated with the integration point. After crack formation, the residual shear stiffness along the plane of the crack is determined through the use of a *shear retention* factor. Its value is affected by the presence of the fibres bridging the two sides of the crack. The shear stiffness is considered to decrease as cracks widen. Therefore, in order to allow for degradation in shear stiffness due to crack propagation, the shear modulus is reduced linearly form full shear retention (i.e. no degradation) at the cracking strain to 10% of that at the ultimate tensile strain. It is worth noting that the shear retention does not diminish altogether due to the presence of the fibres which enhance dowel action as well as aggregate interlock by reducing crack opening. Crucially, the fibres contribute to shear resistance by providing tensile resistance (across the crack) to the shear induced *diagonal tension* stresses.

4. Case studies investigated

A series case studies (employing NLFEA) were carried out to validate the numerical results obtained using both the Brittle Cracking and the Damaged Plasticity concrete models available in ABAQUS (2016) against published experimental data (Zhang *et al.*, 2014, Behinaein *et al.*, 2016). To assess the ability of the NLFEA models developed to accurately predict SFRC *material* behaviour, the first case study considered examines the behaviour of a notched SFRC beam (without conventional reinforcement) when subjected to static and impact loading. The behaviour of these specimens was originally established experimentally by Zhang *et al.* (2014). Consequently, in order to ascertain the ability of the NLFEA models developed to predict the behaviour of SFRC *structural* elements (with conventional reinforcement), a comparative study focusing on investigating the behaviour of SFRC beam specimens under static and impact loading was carried out. The behaviour of these specimens was investigated experimentally by the authors as part of the present study. The validated predictions obtained were then used to study the effect of steel fibres on the behaviour of SFRC at both the *material* and *structural* levels under static and impact

loading conditions. The aforementioned studies are subsequently followed by a parametric study. The behaviour of the RC beam specimens, that form the subject of the parametric study, has been established experimentally by Hughes and Spiers (1982) and numerically by Cotsovos and Pavlović (2012) under both static and impact loading. The comparison of the numerical predictions with the available test data confirmed the ability of the NLFEA model employed to realistically predict RC structural response under both low and high rate loading. Subsequently, fibres were added to the beams and a comparison between the RC and SFRC counterparts was carried out. The numerical predictions obtained were focused on assessing the effect of fibres on the behaviour of the beam specimens considered herein when subjected to impact loads characterised by different loading rates. The numerical studies were also used to address a common shortcoming in impact experimental studies, which usually lead to the complete destruction of the specimen and often display *post*-failure characteristics of little value in terms of design. To address this, the impact loading was applied gradually in pulses in order to pin-point the *actual* failure point. This is useful in determining the load-carrying capacity of the beam. To achieve this, the imposed impact load was assumed to be described by a simplified force-time function which consists of an ascending and descending branch in which the rate of loading (associated with the ascending branch) is considered equal to the rate of unloading (associated with the descending branch).

5. Notched SFRC beam

As explained earlier, the notched beam specimens tested by Zhang *et al.* (2014) were chosen in the present numerical study to investigate the responses of SFRC at the *material* level under low and high-loading rates. The beam was reinforced with hooked-end steel fibres provided at a volume fraction of $V_f = 0.8\%$. The dimensions of the beam specimen and the notch induced conform to the RILEM (2003) indirect tensile testing standard for SFRC.

5.1 SFRC beam specimen details

Three-point bending tests under various loading rates were undertaken by Zhang *et al.* (2014) on the simply-supported SFRC beam depicted in Fig. 2. The properties of steel fibres and concrete strengths are summarised in Table 1 and no other form of reinforcement was provided. The beams were notched at the centre with a notch-to-depth ratio of around 1/6. The behaviour of the specimens was initially established under static loading applied monotonically to failure. The specimens were then subjected to drop-weight tests to establish their behaviour under impact loading using a hammer weighting 120.6 kg dropped from three different drop weight heights of 40 mm, 160 mm and 360 mm in order to achieve three different values of impact velocity of 8.85×10^2 mm/s, 1.77×10^3 mm/s and 2.66×10^3 mm/s, respectively. The heights were chosen so that the maximum impact energy - i.e. the one associated with drop height of 360 mm - was not enough to destroy the beam completely and thus allowing a detailed study of the fracture processes exhibited by the SFRC (as opposed to studying *post*-failure mechanisms commonly associated with specimens tested under impact loads which led to their complete destruction and thus rendering the corresponding results of little practical use).
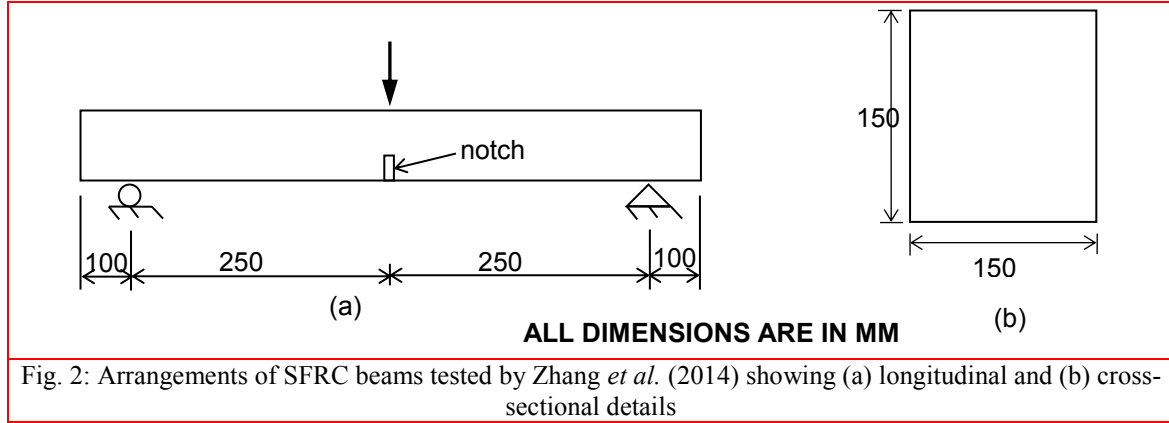
Fig. 2: Arrangements of SFRC beams tested by Zhang *et al.* (2014) showing (a) longitudinal and (b) cross-sectional details

Table 1: Summary of design parameters characterising SFRC beams tested by Zhang *et al.* (2014)

Fibre type	Length (l) [mm]	Diameter (d) [mm]	Fibre volume fraction (V_f) [%]	Compressive strength (f_{ck}) [MPa]	Tensile strength (f_{tk}) [MPa]
Hooked-end	35	0.75	0.8	76	5.1

5.2 Numerical results for SFRC beam under static and impact loading

Fig. 3 shows the tensile stress-strain constitutive relationship proposed by Lok and Xiao (1999), which was incorporated into both the Brittle Cracking and the Damaged Plasticity concrete models presently employed for describing concrete material behaviour. As explained earlier, the former model is a simple one with few parameters and is suitable for materials which are fundamentally affected by brittle cracking such as concrete in flexure. In contrast, the more elaborate Damaged Plasticity model has more parameters to calibrate. The comparison between the experimental data under the static load and the numerical counterparts is depicted in Fig. 4. The load-deflection curves show that both concrete models adopted, adjusted using Lok and Xiao (1999) continuative model for SFRC, provide predictions which are in good agreement with the experimental data. To examine the behaviour exhibited under impact loading, a comparison was performed between experimental and numerical results describing the variation of the dynamic increase factor (DIF) expressed as the ratio between the maximum sustained load *maxP_d* and the load-bearing capacity established under static loading *maxP_s*, under increasing loading rates as presented in Fig. 5. The results show that the use of both concrete material models provided predictions that are in good agreement with the available experimental data.
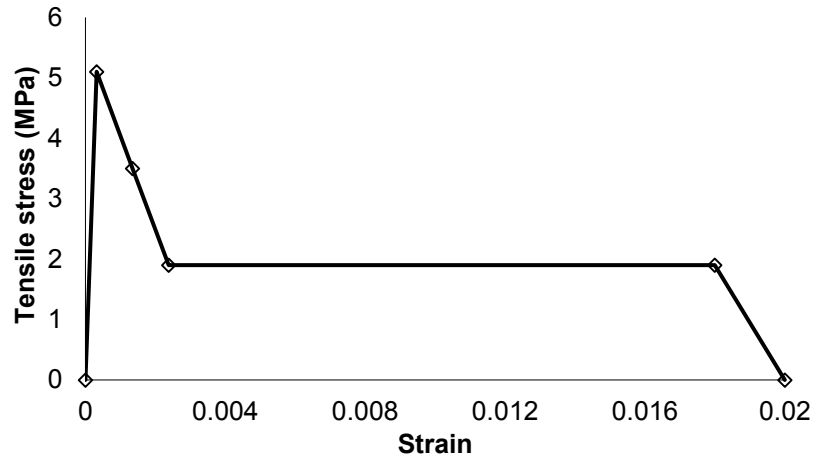
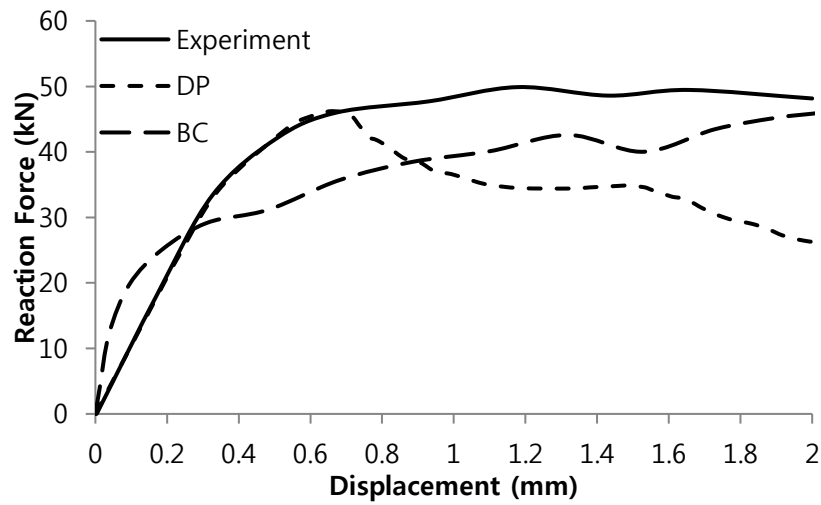Fig. 3: Tensile stress-strain diagram adopted for modelling the beam tested by Zhang *et al.* (2014) with V_f = 0.8%

Fig. 4: Comparison between experimental and numerical results for the static load-deflection curve of SFRC beam tested by *Zhang et al.* (2014)

Fig. 5: Comparison between experimental and numerical impact results of $maxP_d/maxP_s$ for SFRC beam tested by Zhang *et al.* (2014)
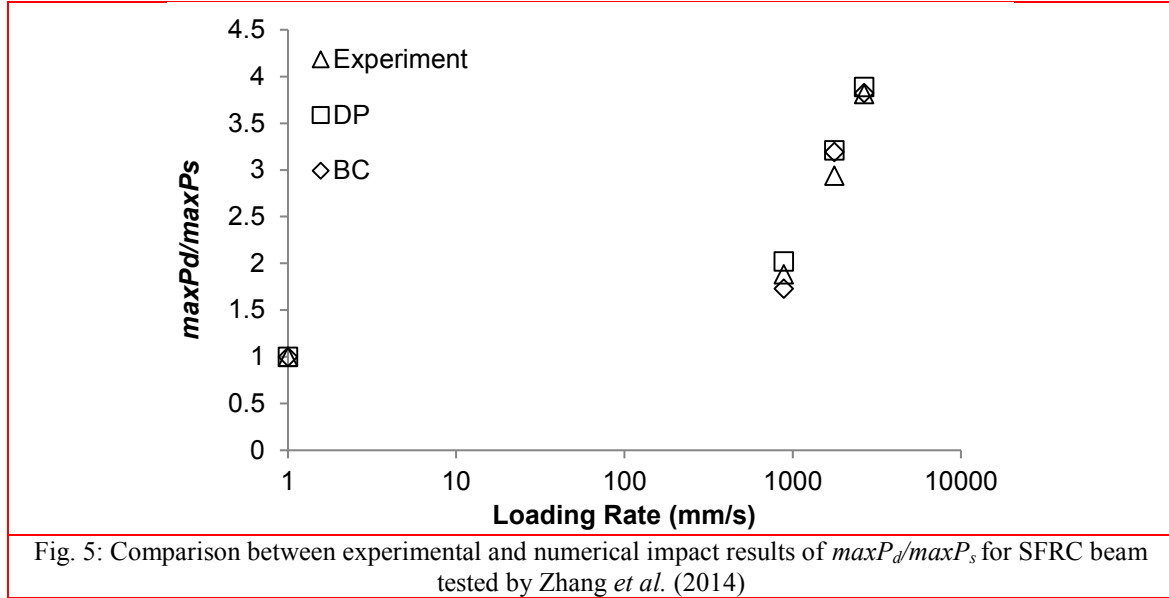
Figs 6 (a-c) shows the comparison between the predictions describing the variation of the generated reaction forces with time and mid-span deflections obtained using both ABAQUS Brittle Cracking and Damaged Plasticity models, and their experimentally established counterparts for the different loading rates considered. Good agreement is observed between the numerical results and the experimental data, with both predictions obtained from the Brittle Cracking and Damaged Plasticity models providing similar results. Figs 7 (a-d) shows the contours of principal strains on the beam under static loading as well as at different rates of impact loading (with the latter modelled using a striker) prior to failure. The data essentially shows the extent of the damage sustained by specimens prior to failure when considering different loading rates. The tensile strain that causes fibre pull-out of 0.02 is also highlighted, which shows that wider and deeper cracks are caused at higher loading rates. The presence of fibres seems to have expanded the region affected by the impact load. Crucially, it has allowed for the development of wider cracks that penetrate to the compression zone than in the case of static loading, indicating that the fibres have helped ensure the development of a more ductile flexural failure mode. Figs 8(a-c) depicts the deflected shapes of the beam when the maximum contact force, maximum reaction force were reached as well as the maximum deflection at failure (i.e. at ultimate force) for different loading rates. The data shows the effect of the lag between contact and reaction forces on one hand and the ultimate force on the other. The significant difference in deflection values (especially the peak one at the centre of the beam) demonstrates the ductility and the slowing of the impact stress wave due to the fibres.
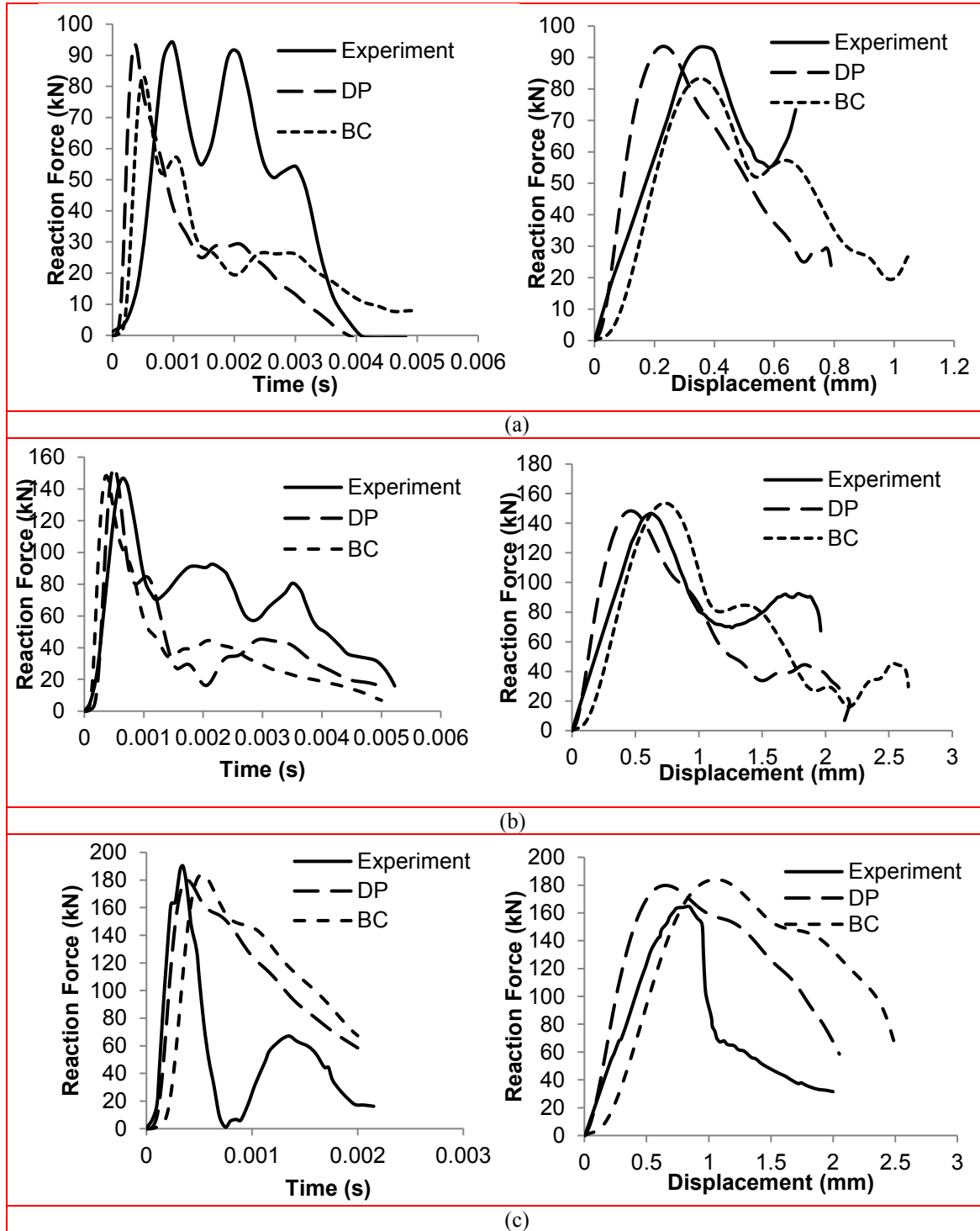
Fig. 6: Comparison between reaction forces versus time (left) and reaction force versus displacement (right) for experimental, Damaged Plasticity (DP) and Brittle Cracking (BC) numerical models results at loading rates (a) 8.85×10^2 mm/s, (b) 1.77×10^3 mm/s and (c) 2.66×10^3 mm/s for Zhang *et al.* (2014) beams
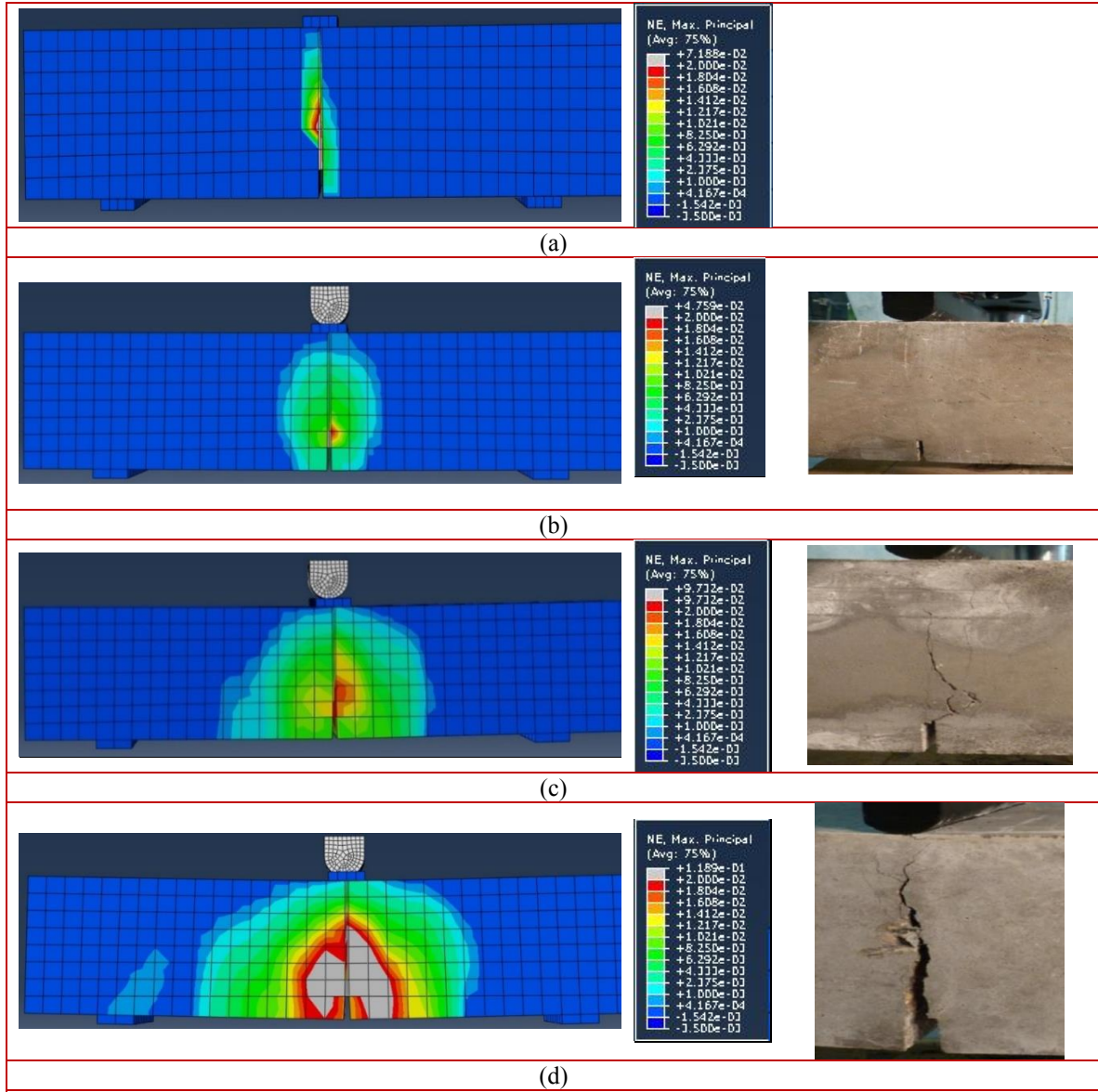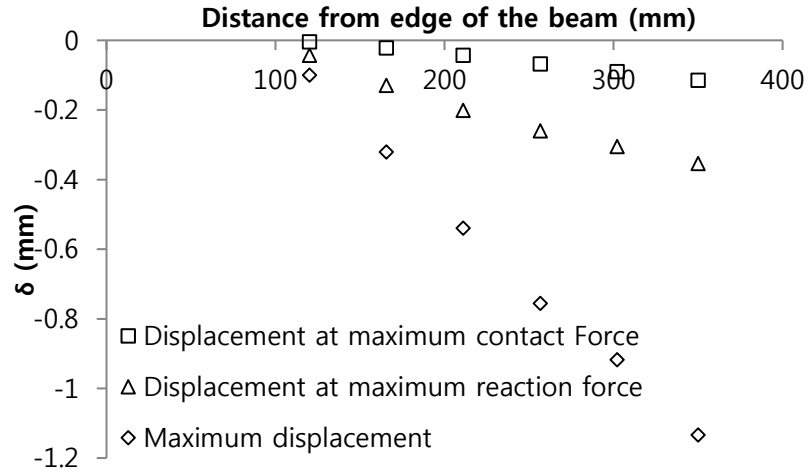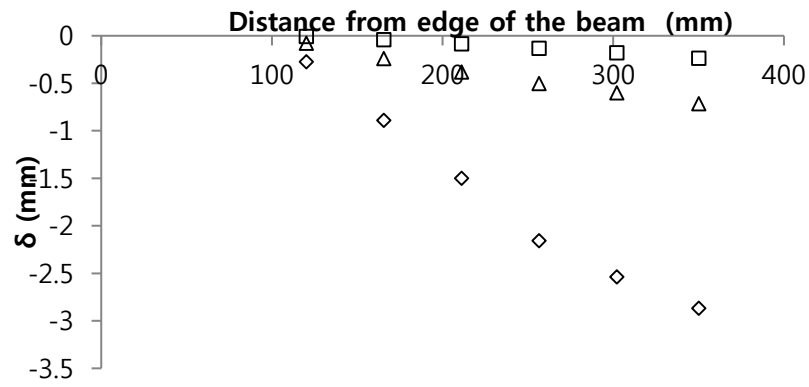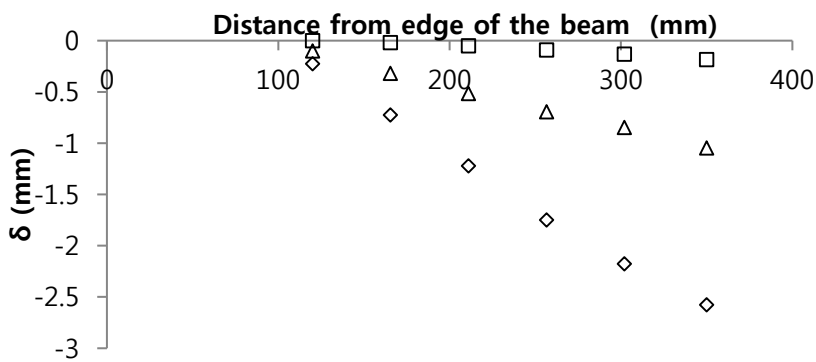
Fig. 7: Principal strain distribution along SFRC beam for loading rates (a) static loading (b)8.85×10^2 mm/s, (c)1.77×10^3 and (d) 2.66×10^3 mm/s compared with cracking patterns from Zhang *et al.* (2014)

Fig. 8: Deflected shapes at the maximum contact force, maximum reaction force and maximum defl ection (i.e. failure) for loading rates (a) 8.85×10^2 mm/s, (b) 1.77×10^3 mm/s and (c) 2.66×10^3 mm/s for Zhang *et al.* (2014) beams

6. SFRC beam with conventional reinforecement

A simply-supported concrete beam was tested as part of the present research work under both static and impact loading. The beam was reinforced with conventional longitudinal and transverse steel bars and both RC (i.e. without fibres) and SFRC cases were tested in order to provide insight into the role of steel fibres. The beam span was chosen so that it enables the investigation of the responses at the *structural* level under impact loading, as the beam dimensions are more substantial than those considered in the preceding case study (at the *material* level using Zhang *et al.* (2014) beam). The experiential study was complimented with a numerical investigation to help validate the numerical model and understand the structural responses in more detail.

6.1 RC/SFRC beam specimen details

Simply-supported concrete beams with spans of 1.3 m were fabricated and the structural behaviour of the beams was experimentally established by conducting static as well as drop-weight tests. During drop-weight testing a 124 kg steel impactor was allowed to fall on the beam specimens at their mid-span from heights of 1.5 m and 2.5 m, resulting in two different values of impact velocity of 54.25×10^2 mm/s and 70.04×10^2 mm/s, respectively. Initially RC (i.e. without fibres) beams were tested and then fibres were added at a volume fraction $V_f = 1\%$. The shape and geometry of the beam specimens are shown in Fig. 9. Steel bars with diameters 12 and 8 mm were used, which had a modulus of elasticity of $E_S = 200$ GPa, whilst the remaining material properties of concrete, fibres and steel bars are summarised in Table 2.
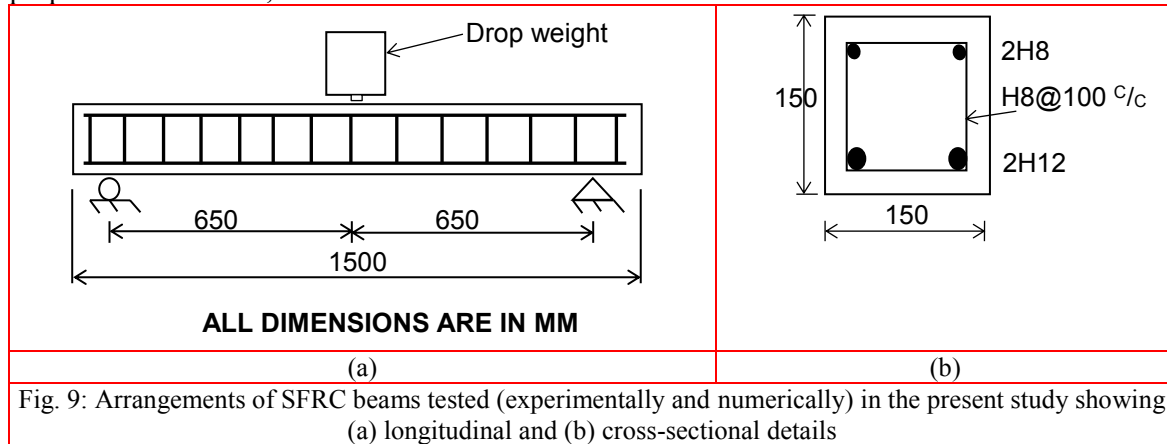

Fig. 9: Arrangements of SFRC beams tested (experimentally and numerically) in the present study showing (a) longitudinal and (b) cross-sectional details

Table 2: Summary of material properties characterising (a) SFRC and (b) steel bars for beams tested in the present study

Fibre type	Length (l) [mm]	Diameter (d) [mm]	Aspect Ratio (l/d)	Compressive strength (f_{ck}) [MPa]	Tensile strength (f_{tk}) [MPa]
Hooked-end (3D)	50.0	1.05	45	30	2.91

(a)

Rebar Size (mm)	12	8
Yield strength $f_y(MPa)$	517	503
Ultimate strength $f_u(MPa)$	667	640
Yield strain ε_y	0.002125	0.002515
Ultimate strain ε_u	0.095	0.11

(b)

## 6.2 Numerical results for RC/SFRC beam under impact loading

Fig. 10 shows the comparison between the experimental and numerical results obtained under static loading for beams with and without fibres. It can be seen that the numerical results (using both ABAQUS Brittle Cracking and Damaged Plasticity concrete models) are in good agreement with the experimental results. The results show that the Brittle Cracking model, despite its simplicity, can provide accurate results (especially for cases where the response is dominated by tensile failure such as beams presently used). The data also shows that the addition of the steel fibres at a dosage of $V_f = 1\%$ led to an enhancement in both the strength and maximum deflection (increasing by ~32% from 38 kN to 50 kN and ~15% raising from 35 mm to 40 mm, respectively). Fig. 11 shows the comparison between experiential and numerical results of the beams under impact loading for the two loading rates considered. The comparison is based on the use of the $maxP_d/maxP_s$ ratio and the results show that the use of both concrete material models provided predictions that are in good agreement with the experimental data. Fig. 12 shows the distribution of principal strains, which was used to illustrate the cracking patterns at failure. The strain contours' intervals were selected to reflect the material characteristics (so in tension a grey colour was used to represent strains at cracking strain for RC beams and the strains at pull-out failure for SFRC beams, whilst in compression dark colour close to black was used to represent the crushing strain). The figures show good agreement between the cracking patterns captured experientially and their numerical counterparts. For the low-rate (i.e. static) loading, the cracks propagate along the entire beam from the point of applying the load to the support. On the other hand, as the loading rate is increased, the cracked zone decreases until it becomes more localised around the applied impact load (with the rest of the beam remaining largely unaffected). This shows that as the rate of loading increases, the portion of the beam span mostly affected by the applied load reduces. The cracking patterns also show that the addition of fibres has led to a better control of cracks (with hardly any pull-out failure) resulting in a more ductile response and allowed for the development of finer cracks in a wider zone. So the fibres seem to have allowed for an increase in the localised zone around the impact load observed earlier. Figs 13(a-d) depicts the deflected shapes of the beam when the maximum contact force, maximum reaction force were reached as well as the maximum deflection at failure, i.e. at ultimate force, for the loading rate associated with drop heights of 1.5 m and 2.5 m. The results show the delay between the contact and reaction forces indicating the ductility provided by the fibres and bars (this is clear also from the marked difference between deflections at failure and those measured at peak contact force. This along with the cracking patterns presented earlier show that the fibres allow for better energy absorption, which is important for impact-resistant design.
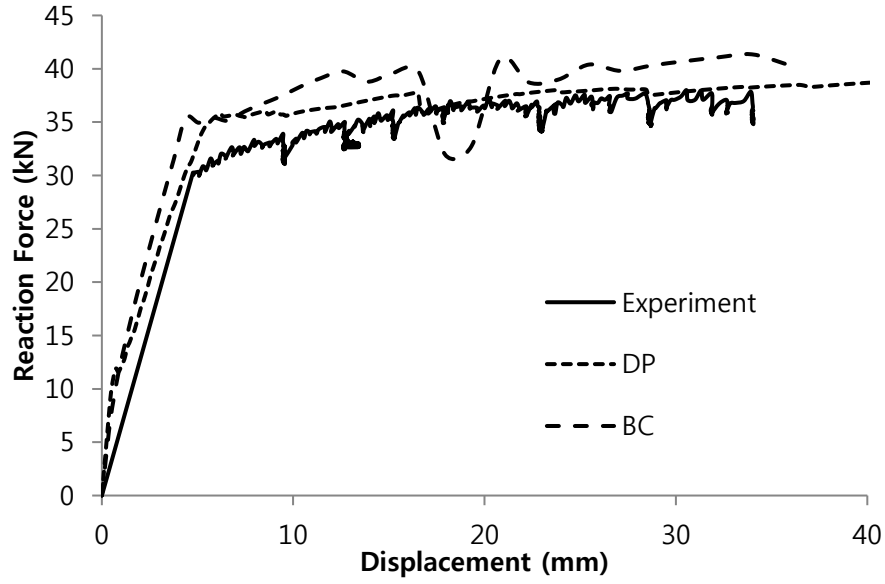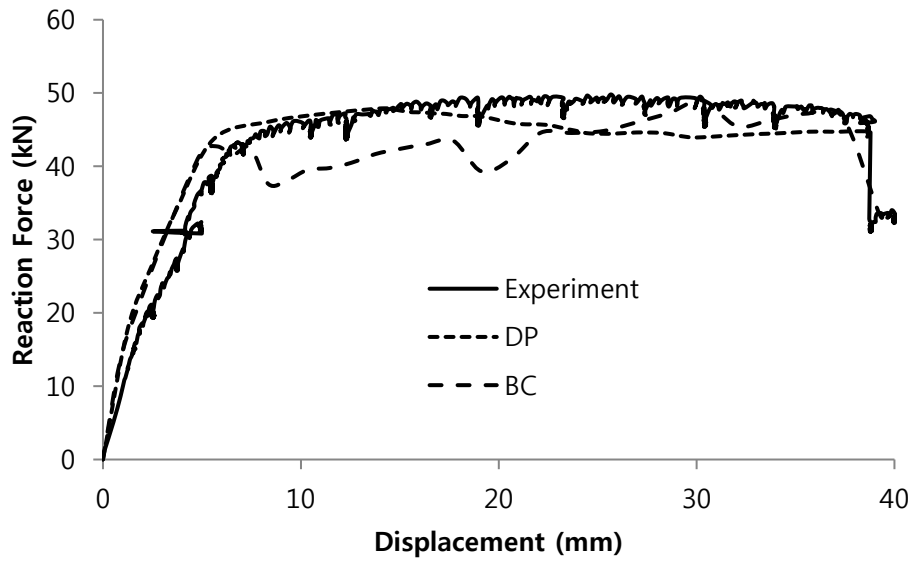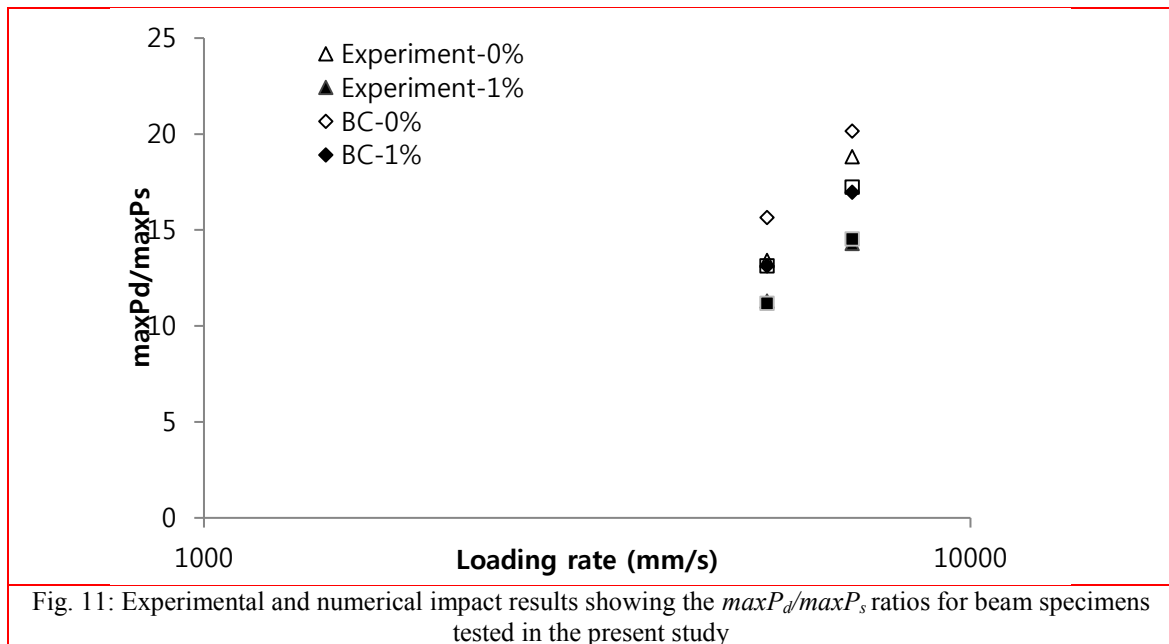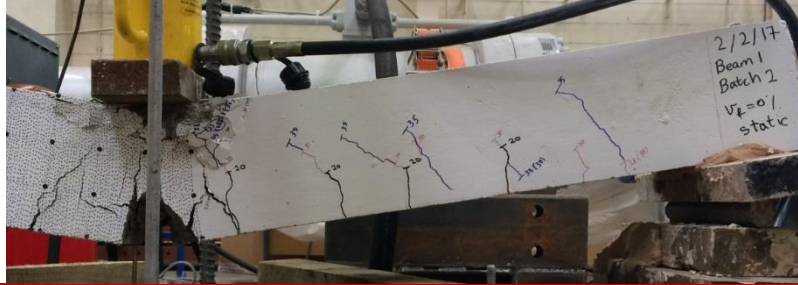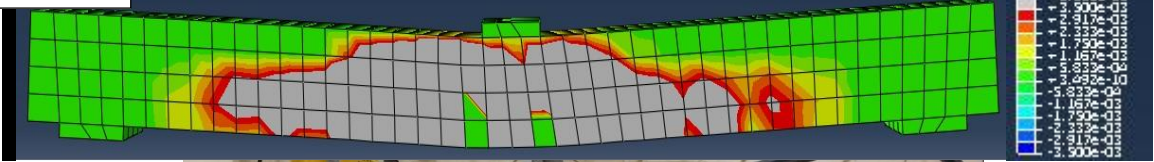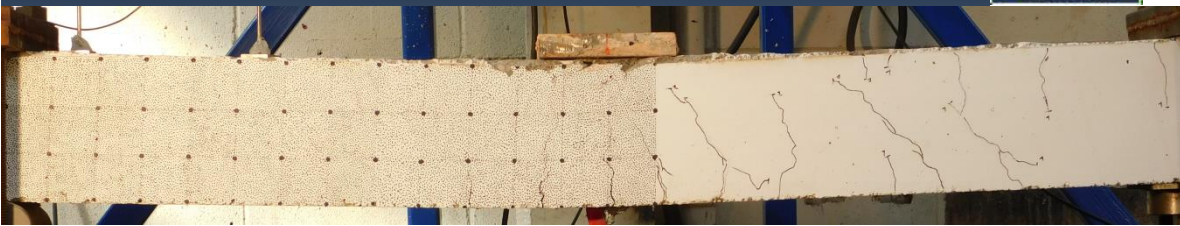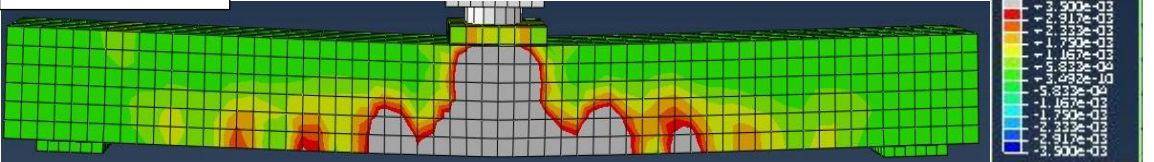
Fig. 10: Load-deflection curve obtained experimentally and numerically by testing the specimens under static loading monotonically applied to failure with fibre content of (a) $V_f = 0\%$, and (b) $V_f = 1\%$

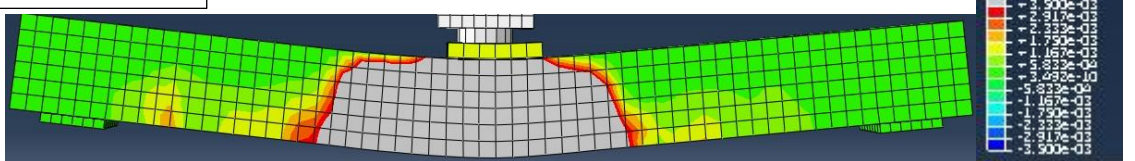Fig. 11: Experimental and numerical impact results showing the $maxP_d/maxP_s$ ratios for beam specimens tested in the present study
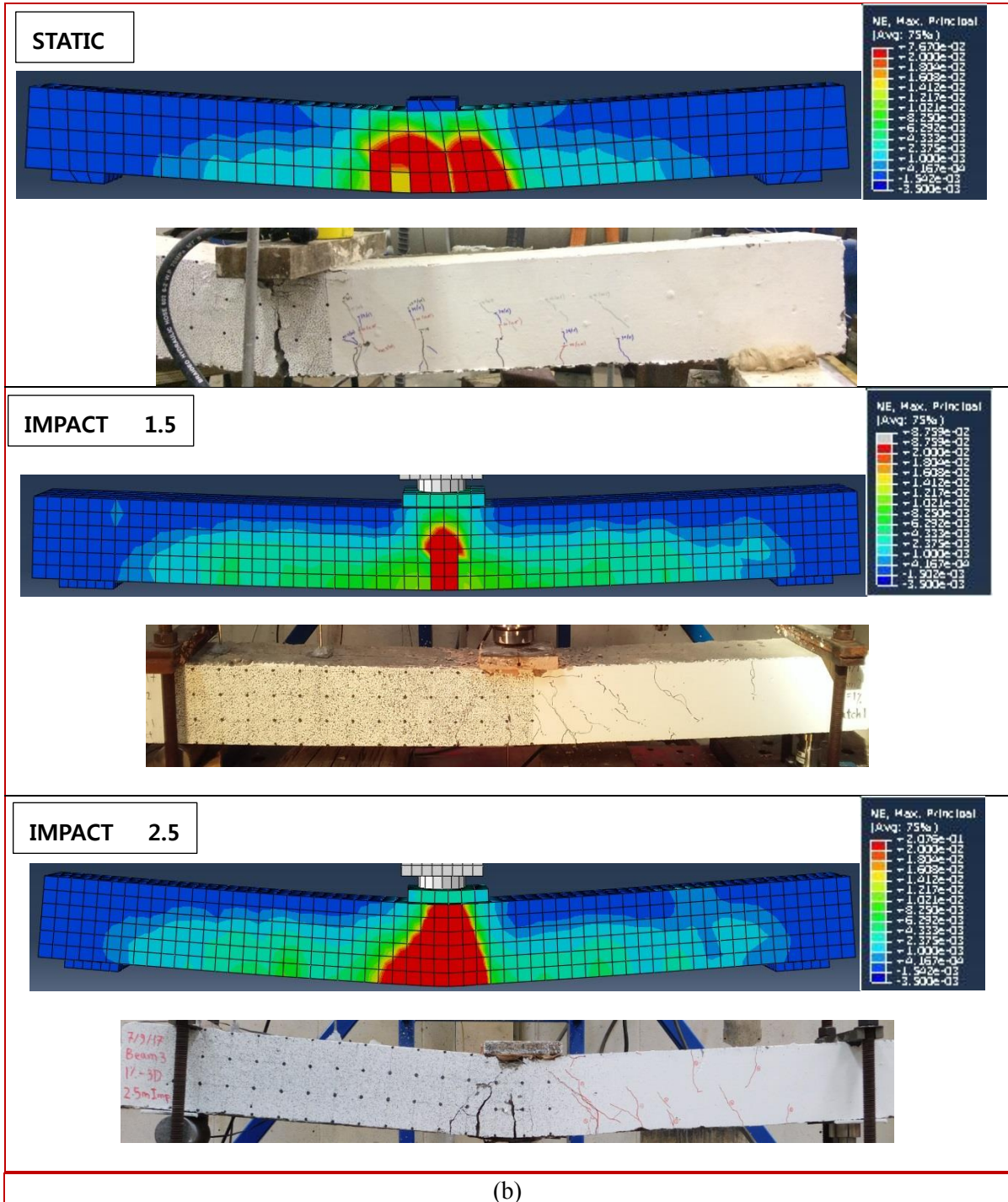
STATIC
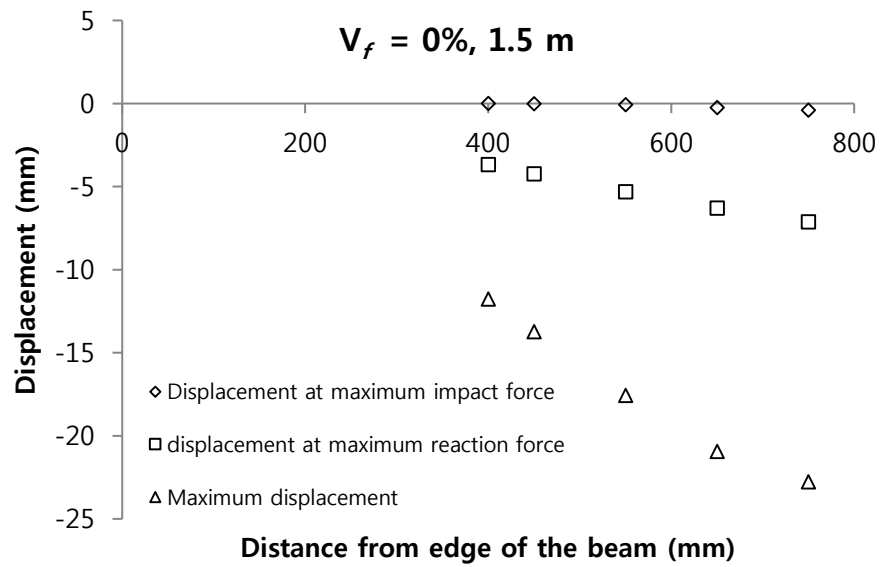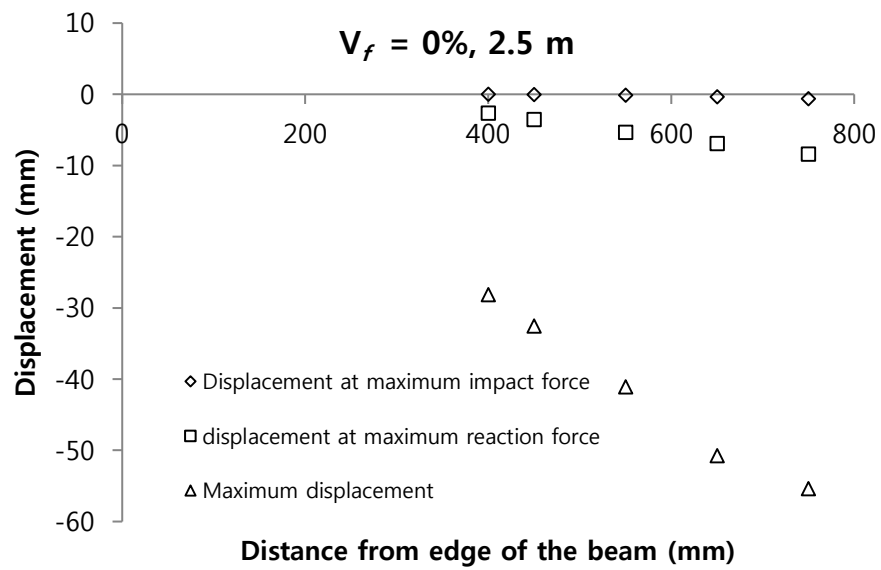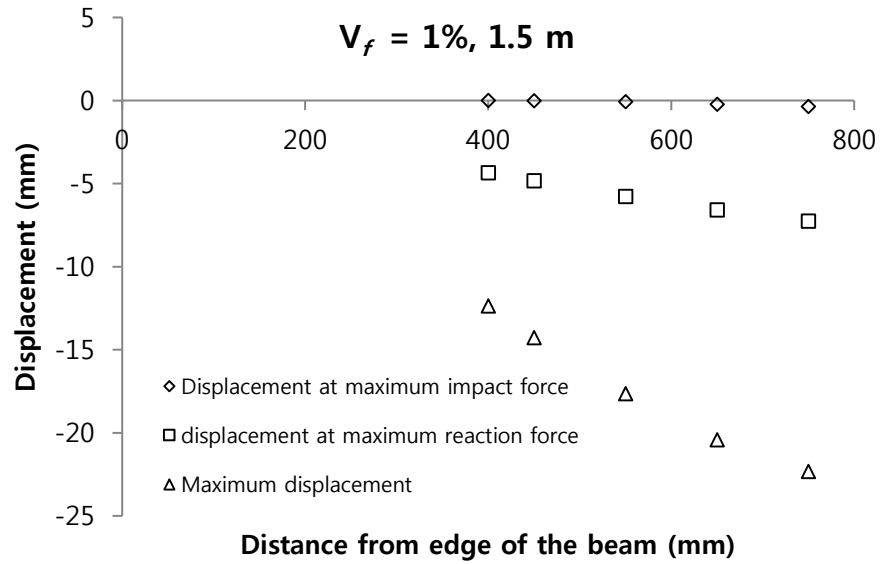
IMPACT 1.5 m

IMPACT 2.5 m

(a)

Fig. 12: Principal strain distribution along SFRC beam under static and impact loading after 1st drop from two heights (1.5 m and 2.5 m) for beams with fibre content of (a) V$_f$ = 0%, and (b) V$_f$ = 1%

V_f = 0%, 1.5 m

Displacement (mm) [y-axis]

Distance from edge of the beam (mm) [x-axis]

◇ Displacement at maximum impact force
□ displacement at maximum reaction force
△ Maximum displacement

(a)

V_f = 0%, 2.5 m

Displacement (mm) [y-axis]

Distance from edge of the beam (mm) [x-axis]

◇ Displacement at maximum impact force
□ displacement at maximum reaction force
△ Maximum displacement
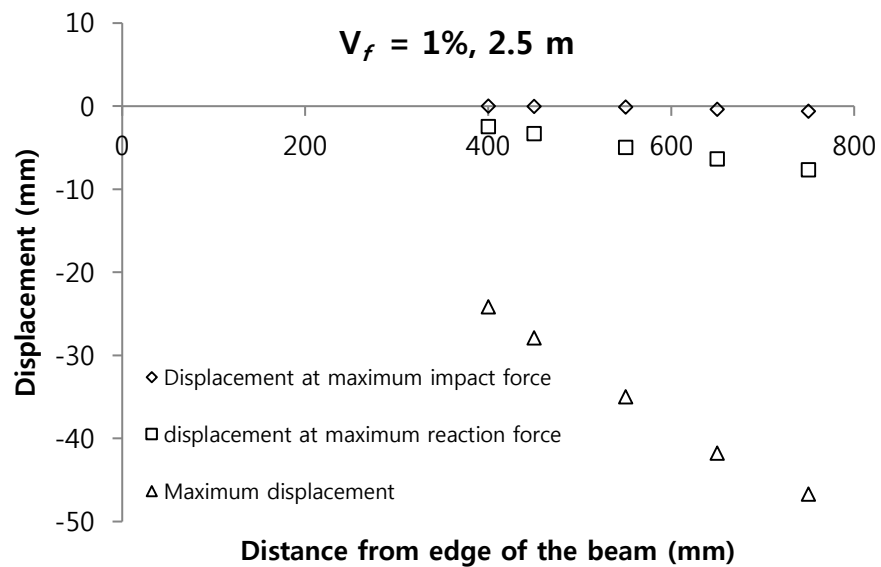
(b)

Figs 13: Deflected shapes at the maximum impact force, maximum reaction force and maximum deflection for RC beams (without fibres) after 1st drop from heights of (a) 1.5 m, (b) 2.5 m and for SFRC beams (with V_f = 1%) from heights of (c) 1.5m and (d) 2.5m impact

7. Parametric investigation

Initially, the case of RC beam tested by Hughes and Spiers (1982) was modelled using NLFEA under both static and dynamic (i.e. high-rate/impact) loading and subsequently a further study was carried out by adding fibres to this specimen in order to study SFRC under impact (Behinaein *et al.*, 2016). Crucially, the numerical studies were also used to address the shortcoming in the impact experiments as they resulted in the complete destruction of the specimen and thus produced *post-failure* characteristics of little value in terms of design. Therefore, in the numerical studies, the impact loading was applied gradually in pulses in order to pin-point the *actual* failure point and consequently the load-carrying capacity of the beam.

7.1 RC beam specimen details

The behaviour of the RC simply-supported beam considered herein has been experimentally investigated by Hughes and Spiers and termed specimen C2 in the original tests by Hughes and Spiers (1982) under static and impact loading. The specimen was designed to undergo a ductile (i.e. flexural) failure mode. The details of beam specimen are depicted in Fig. 14. The modulus of elasticity E_S, the yield stress f_y and the ultimate strength f_u of both the longitudinal and transverse reinforcement bars are 206 GPa, 460 MPa and 560 MPa, respectively. Concrete cover to reinforcement of 25 mm was provided throughout the beam. The uniaxial compressive strength f_c of concrete is 45 MPa. The beams were subjected to drop weight testing at their mid-spans. Mild steel, rubber or ply pads were placed on the top face of the specimen in order to prevent or moderate local damage in the impact area and to some extent control the rate of loading.
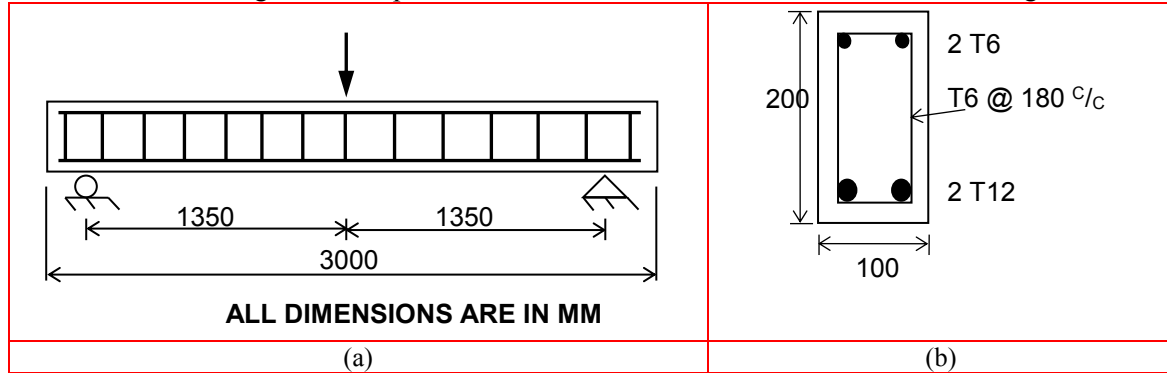

(a)	(b)

Fig. 14: Arrangements of RC beam investigated numerically (adopted from specimen C2 tested by Hughes and Spiers 1982) showing (a) longitudinal and (b) cross-sectional details

7.2 Numerical results for RC beam under static loading

Nonlinear FE analysis was carried using 3D brick elements with a mesh size of 20 mm as depicted in Fig. 15a. Owing to the symmetrical geometry of the beam, only a quarter of the beam was modelled and small steel plates were provided at support and loading points to mimic the experimental setup and help avoid pre-mature localised numerical failure. The tensile cracking strain of concrete was considered to be 0.001 and the shear retention factor was taken as 0.1. The analysis was carried out using both Brittle Cracking and Damaged Plasticity model, considering the specimen under static and different high rate loading. The comparison between the FE-based

predictions and experimental results for the static load case are presented in Fig. 15b, which shows that there is reasonable agreement between the ensuing load-deflection curves for both ABAQUS concrete models considered.
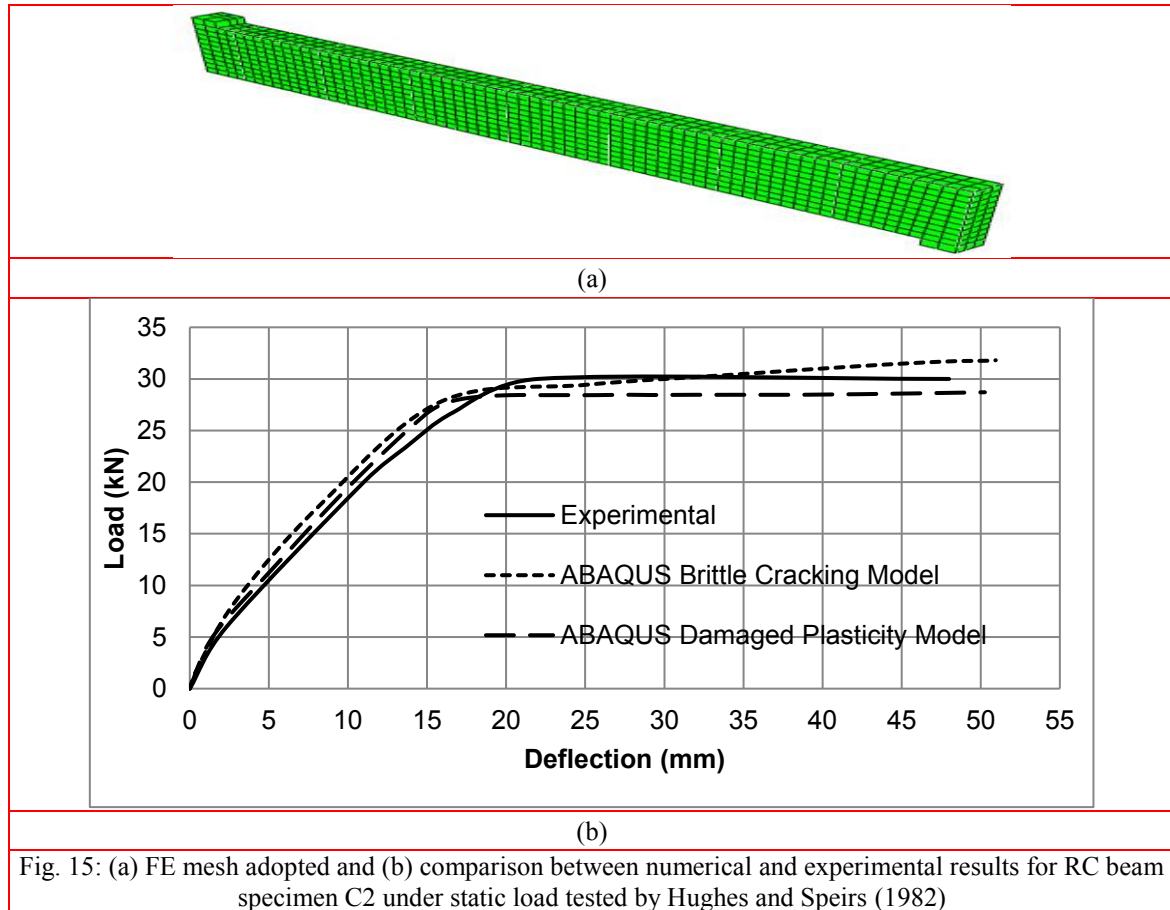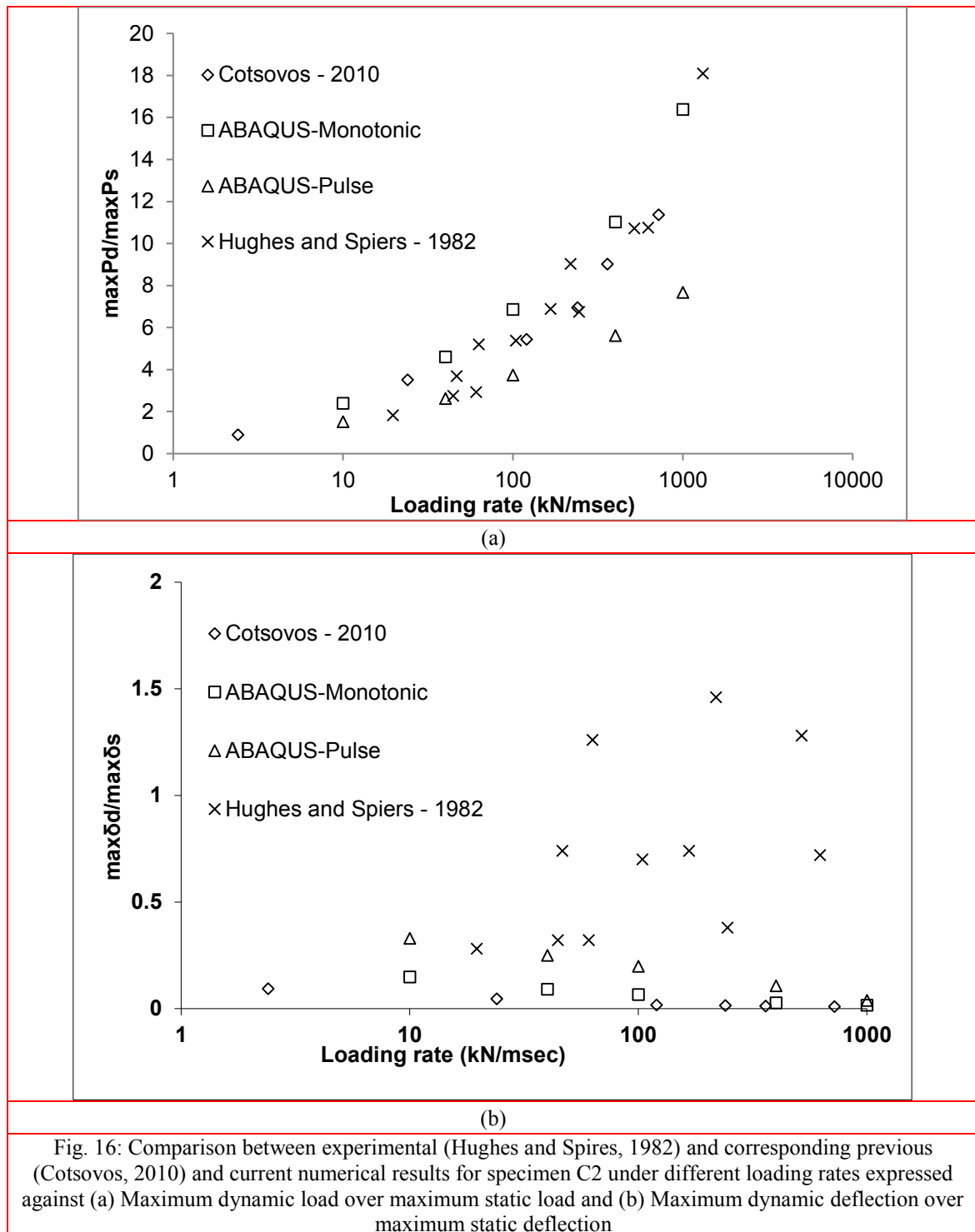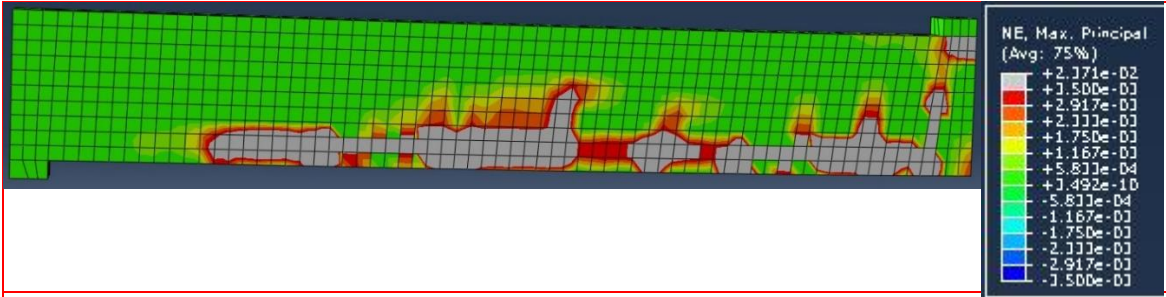

(a)

(b)

Fig. 15: (a) FE mesh adopted and (b) comparison between numerical and experimental results for RC beam specimen C2 under static load tested by Hughes and Speirs (1982)

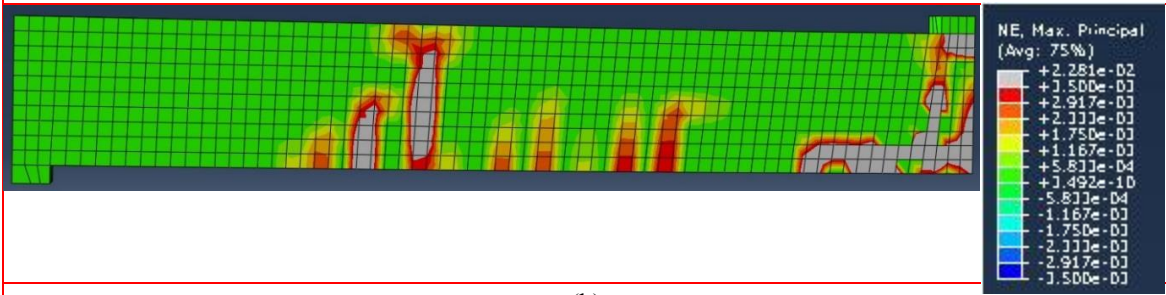### 7.3 Numerical results for RC beam under impact loading

For the impact test case, the results obtained as the maximum dynamic load and deflection over static load are compared with the corresponding experimental and numerical results of Hughes and Speirs (1982) and Cotsovos (2010) as depicted in Figs 16(a-b). Different loading rates were considered in the numerical study ranging from 10 to 1000 kN/msec, which were applied once monotonically and then in the form of a pulse load. The pulse load was applied in different stages, initially using the value of the maximum load sustained monotonically and consequently that load was reduced every time by 10% (of the maximum monotonic load sustained). The reduction continued in this manner to the point that the beam can bear the applied load, as shown in Fig. 1. The aim was to determine the *actual* load-carrying capacity as the load applied during the experimental testing led to the complete destruction of the specimen and hence was not useful in determining the load-carrying capacity of the specimen. This is a common shortcoming of

experimental testing under high rates of loading and limit its usefulness in terms of *design*, where a containment is needed up to a certain load threshold. To address this, the NLFEA-based study considered applying in the reduced pulse manner described in order to help pinpoint the actual failure point and determine the all-important load-carrying capacity value. The variation of the dynamic increase factor (DIF) was considered as depicted in Fig. 16(a), i.e. the maximum load sustained by the RC beams under high rate loading normalised with respect to its counterpart under static loading $maxP_d/maxP_s$, which shows a good correlation between the experimental and numerical results. Another indicator of the DIF was also considered in Fig. 16(b), namely the ratio between the maximum displacement at mid-span under the dynamic load and the corresponding displacement under static load $Max\delta d/Max\delta s$. Even though the experimental results of the latter are scattered, both current and previous numerical data show good agreement with each other and are within the scatter range of experiential results (on the safe side). The $Max\delta d/Max\delta s$ results also show that an increase in the loading rate leads to an increase in stiffness and load-carrying capacity combined with a decrease of the maximum deflection at mid-span. The responses of the monotonic and pulse loading methods of application show that the actual failure (i.e. pulse) load is approximately two thirds of the impact load recorded in the experiment. A similar conclusion can be made with regards to the central deflection. The discrepancy between the responses (i.e. strength and stiffness) of the two loading application methods increases as the loading rate is raised. Indicative deformed shapes and cracking patterns (the latter examined by considering the principal strains contours) of the beam specimen under different pulse load rates at maximum displacement (i.e. failure) are shown in Figs 17(a-e). The strain contours' intervals were selected to reflect the material characteristics (so in tension a grey colour was used to represent strains at cracking strain for RC beams and the strains at pull-out failure for SFRC beams, whilst in compression dark colour close to black was used to represent crushing strain of 0.0035). For the low rates of loading, the deformation and cracking pattern is similar to the static loading case as cracks propagate along the entire beam from the point of applying the load to the support. On the other hand, as the loading rate is increased, the cracked zone decreases until it becomes more localised in the vicinity of the applied impact load with the highest loading rate. This crack propagation shows that beam acts as a reduced span beam with fixed ends forming at a distance from the applied load, and the rest of the beam remain unaffected. This shows that as the rate of loading increases, the length portion of the beam mostly affected by the applied load reduces. For relatively high rates of loading, this *effective* length (L_{eff}) is confined in the region of the beam mid-span extending on either side of the mid-span cross section to a distance marked by the formation of vertical *flexural* cracking initiating at the upper face – as the beam is effectively partially fixed there to the remainder of the beam that is hardly moving – and extending downwards, whereas the remainder of the beam (i.e. the portions extending between the supports and the aforementioned cracking) remains practically unaffected by the applied load. Therefore, under high rates of loading, the beam behaviour is essentially characterized by L_{eff}.

(a)

(b)

Fig. 16: Comparison between experimental (Hughes and Spires, 1982) and corresponding previous (Cotsovos, 2010) and current numerical results for specimen C2 under different loading rates expressed against (a) Maximum dynamic load over maximum static load and (b) Maximum dynamic deflection over maximum static deflection
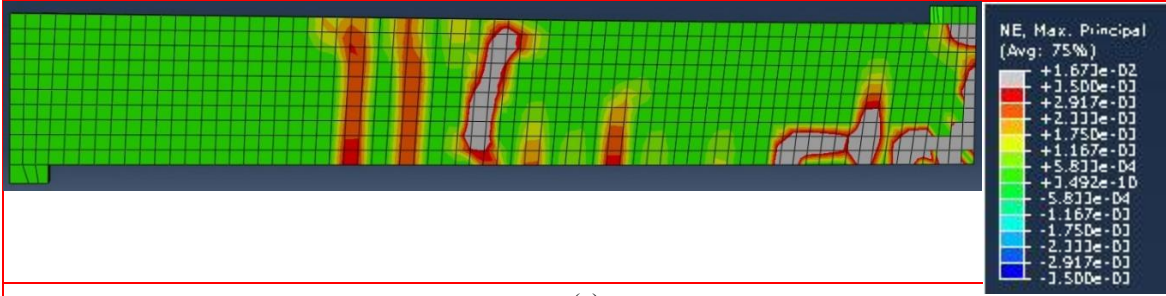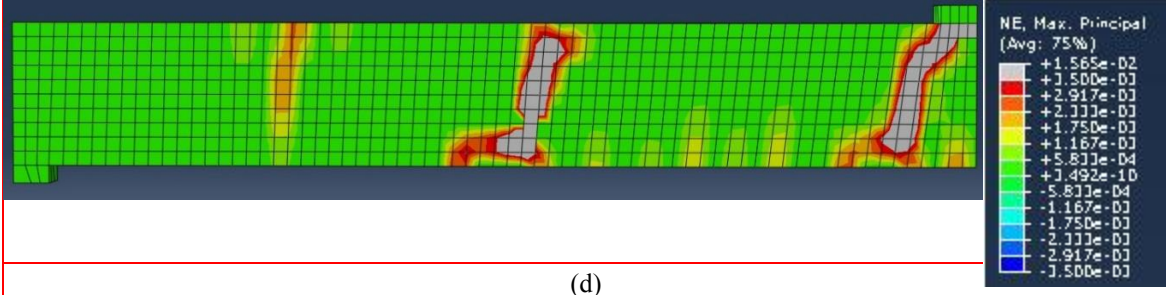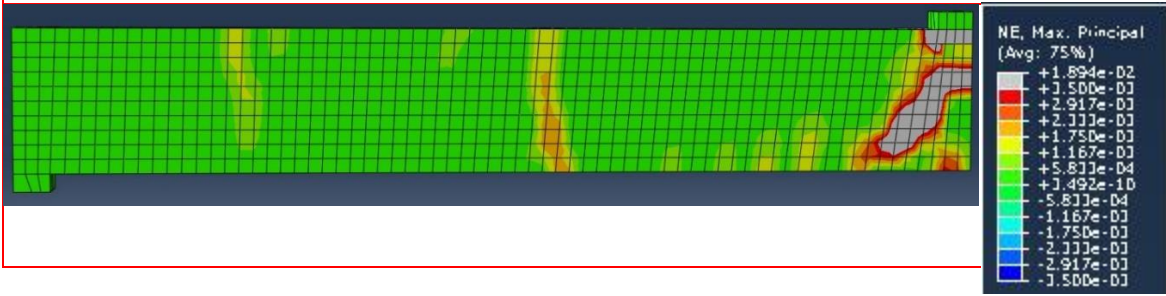
(a)

(b)

(c)

(d)

(e)

Fig. 17: Principal strain distribution along the RC beam at maximum displacement (i.e. failure) for different pulse loading rates (a) 10kN/msec, (b) 40kN/msec, (c) 100kN/msec, (d) 400kN/msec, (e) 1000kN/msec

7.4 Numerical results for SFRC beam under static and impact loading

Following the preceding study by Behinaein *et al.* (2016), of the RC beam specimen C2 tested by Hughes and Spiers (1982) that also served to validate the FE model and strategy used, steel fibres were added with a volume fraction (V_f) value of 1%. The aim of this NLFEA-based study was to enhance understanding of the effect of steel fibres on structural behaviour of RC elements under low and high rates of loading. The material constitutive model proposed by Lok and Xiao (1999) was adopted in order to define the post-cracking tensile stress-strain relationship for SFRC. The load-deflection results under static loading are presented alongside the ones for RC beams (i.e. without fibres) in Fig. 18. The curves were obtained using a displacement-based loading method with incremental displacements applied at the mid-span of the beam. As it is shown, by adding 1% steel fibres to the concrete matrix, both the load-carrying capacity and stiffness were enhanced. The results were extended to include all loading rates considered and the ensuing load-deflection curves for different loading rates are depicted in Fig. 19. The load-deflection curves clearly demonstrate the enhancement in load-carrying capacity and ductility due to the addition of fibres. A comparison between the values of the peak loads and deflections (for RC beams and their counterpart SFRC ones) is summarised in Table 3. The results show that the addition of fibres leads to an increase of both strength and ductility (with the maximum load and deflections used to denote these two key structural performance characterises, which have particular importance for impact-resistant design). The enhancement changes depending on the loading rate applied, ranging from 40% to 74% when the load is applied monotonically (similar trends were found when the load applied as a pulse, i.e. when the actual failure point was sought under impact loading as explained earlier). The enhancement to ductility is as high as 4.8 times the one associated with RC for monotonic loading (and 5.7 for pulse loading). The lowest value for ductility increase due to fibres was found to be ~2.9, which is still a significant improvement. A comparison between the maximum pulse load and the corresponding monotonic load reveals that the *actual* load-carrying capacity is 0.47~0.64 and 0.52~0.70 for RC and SFRC beams, respectively. This suggests that the relevant tests data are associated with *post*-failure behaviour and that the *true* load-bearing capacity of the RC and SFRC beams considered under impact loading is considerably lower than the values recorded experimentally. This, and the potential benefits due to fibres, have useful implications in terms of impact-resistant design. Additionally, the maximum deflection for the pulse load was compared with the monotonic load counterpart. It was found that the ratio between the maximum deflection due to pulse and monotonic loads is 2.23~5.34 and 1.73~7.30 for RC and SFRC beams, respectively. This shows that the pulse load approach captures the *whole* deflection from start of impact until the load pulse becomes zero. This is essential as the beam will continue to deflect under its own *inertial* forces during the unloading phase of the impact load. Thus, the deflections will continue to increase while the striker is rebounding away from the beam. The monotonic approach does not capture this *lag* between the load and deflection. These inertial forces, due largely to the mass of the localised affected zone L_{eff}, could explain the increase in both strength and deflection (and the associated surge in strains) under impact loading. From this viewpoint, the increases are due to the inertial forces of the effective part of the beam rather than due to changes in material properties, such as strain rate dependency.
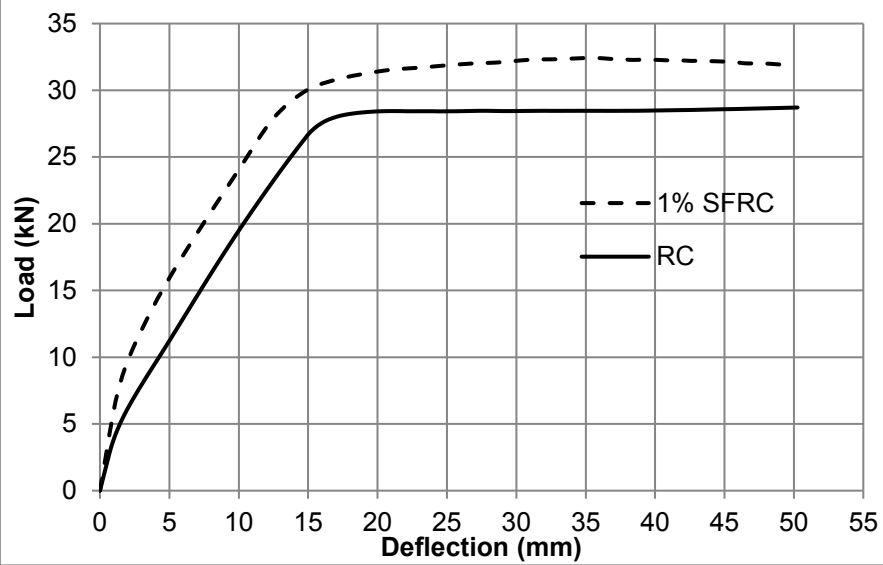
Fig. 18: Comparison between static load-deflection curves in the middle of SFRC and RC beams
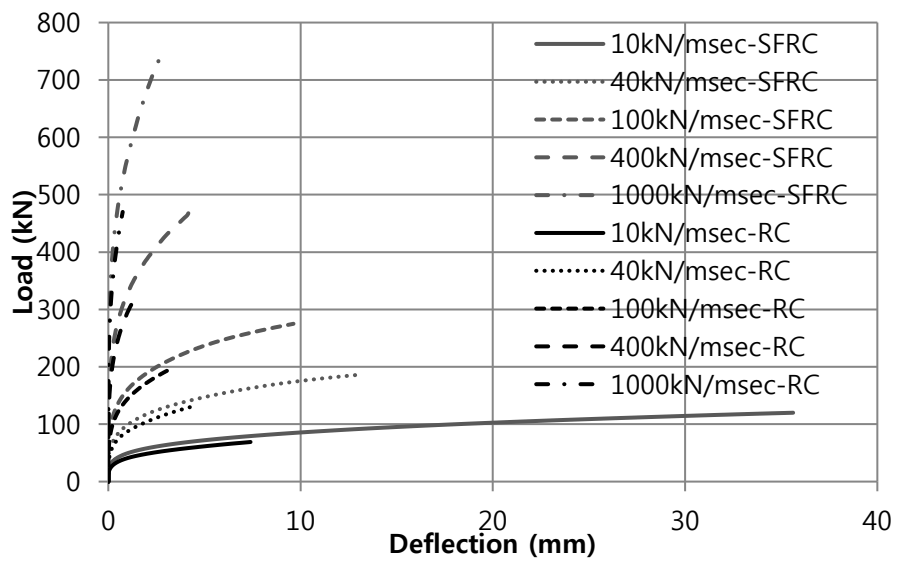

Fig. 19: Comparison between load-deflection curves in the middle of SFRC and RC beams under different loading rates (for monotonic load case)

Table 3: A comparison between strength and ductility values for RC and SFRC beams under (a) monotonic and (b) pulse loading (the maximum load and deflection of the latter is also expressed as ratio of monotonic load)

Loading rate (kN/msec)	Maximum load (kN)			Maximum deflection (mm)		
	SFRC	RC	SFRC/RC	SFRC	RC	SFRC/RC
10	120.00	68.88	1.74	35.62	7.40	4.81
40	186.48	132.16	1.41	13.13	4.51	2.91
100	275.00	197.12	1.40	9.63	3.28	2.94
400	465.84	316.74	1.47	4.17	1.32	3.16
1000	742.50	470.40	1.58	2.73	0.75	3.64

(a)

Loading rate (kN/msec)	Maximum load (kN)			Maximum deflection (mm)		
	SFRC	RC	SFRC/RC	SFRC	RC	SFRC/RC
10	72 (0.60)	43.91 (0.64)	1.64	61.49 (1.73)	16.47 (2.23)	3.73
40	130.54 (0.70)	75.52 (0.57)	1.73	51.81 (3.95)	12.44 (2.76)	4.16
100	181.5 (0.66)	107.52 (0.55)	1.69	41.11 (4.27)	9.9 (3.02)	4.15
400	292.8 (0.63)	161.6 (0.51)	1.81	30.43 (7.30)	5.34 (4.05)	5.70
1000	388 (0.52)	220.5 (0.47)	1.76	14.69 (5.38)	3.83 (5.11)	3.84

(b)

A comparison between the ratios of maximum dynamic to static load-carrying capacity for different rates of loading ($maxP_d/maxP_s$) and maximum dynamic to static displacement ($Max\delta d/Max\delta s$), for both RC and SFRC are shown in Figs 20(a,b), respectively. An increase in load-carrying capacity (and a decrease in the maximum deflection) in the mid-span of the beam is observed for SFRC compared to RC counterparts, which becomes more pronounced as the loading rate is raised. Similar trends were found when the loading was applied as a pulse (i.e. when attempting to pinpoint the actual failure point) as can be seen in Figs 21(a,b), which show that the increase of load-bearing capacity due to the addition of fibres can be as high as three folds for high loading rates. This indicates the potential benefits of fibres in design terms for concrete beams under impact loading. The cracking (examined by considering the principal strains contours) and deformed shape patterns are depicted in Figs 22(a-e), which shows the principal strain distribution along the SFRC beam, at maximum displacement (i.e. failure), for different pulse loading rates ranging from 10 to 1000kN/msec. As pointed out earlier, the grey colour in the contour intervals denotes the pull-out failure region within the beam. The results show that the strains become more localised as the loading rate increased. A comparison between the deflected shapes profiles along both RC and SFRC beams at the maximum contact (i.e. impact) force is depicted in Figs 23(a,b). The results are shown for different loading rates, i.e. 10, 40, 100 kN/msec in Fig. 23(a) and 400 and 1000 kN/msec in Fig. 23(b). It can be seen that the *localised* zone affected by the load (i.e. L_{eff}, which is indicatively shown in the figures) decreases as the loading rate increases. Crucially, however, the fibres help widen this localised zone compared to the one observed in the

corresponding RC beam. Additionally, the fibres enhance the ductility of the beams as evident from the increased deflections and deflected shape profiles of SFRC beams.
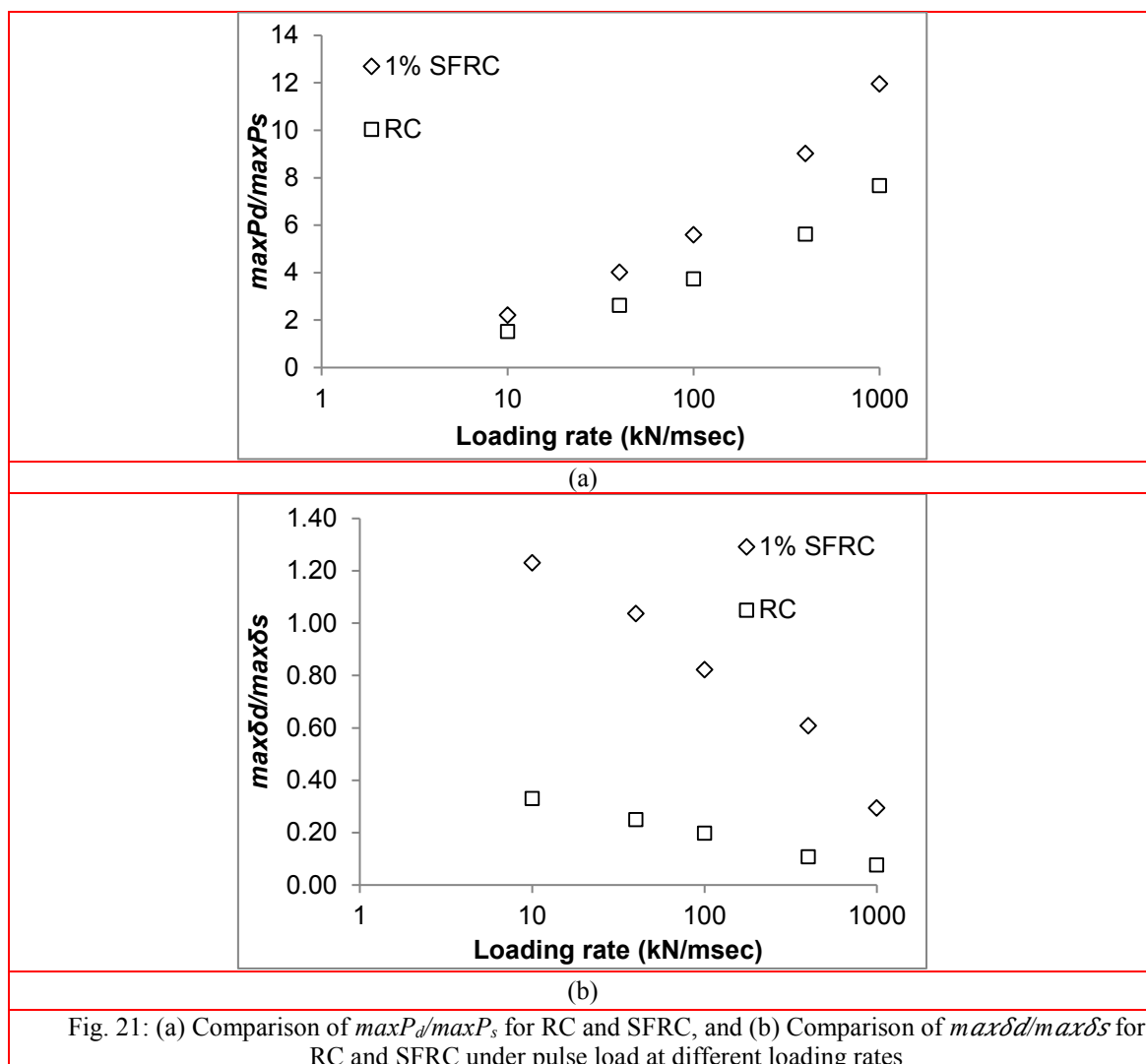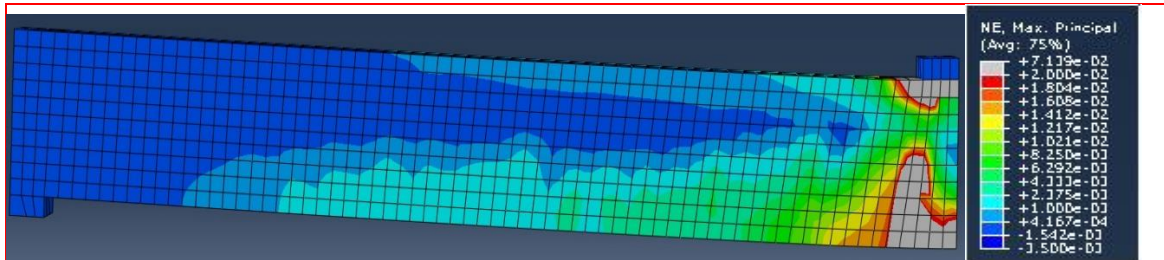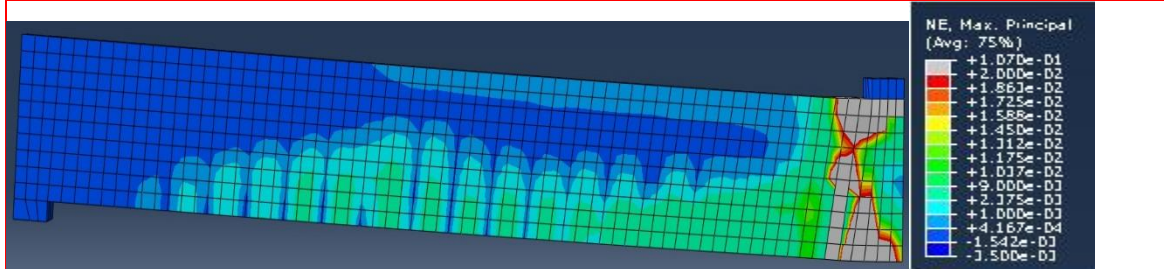

(a)

(b)

Fig. 20: (a) Comparison of $maxP_d/maxP_s$ for RC and SFRC, and (b) Comparison of $max\delta d/max\delta s$ for RC and SFRC under monotonic load at different loading rates

(a)

(b)
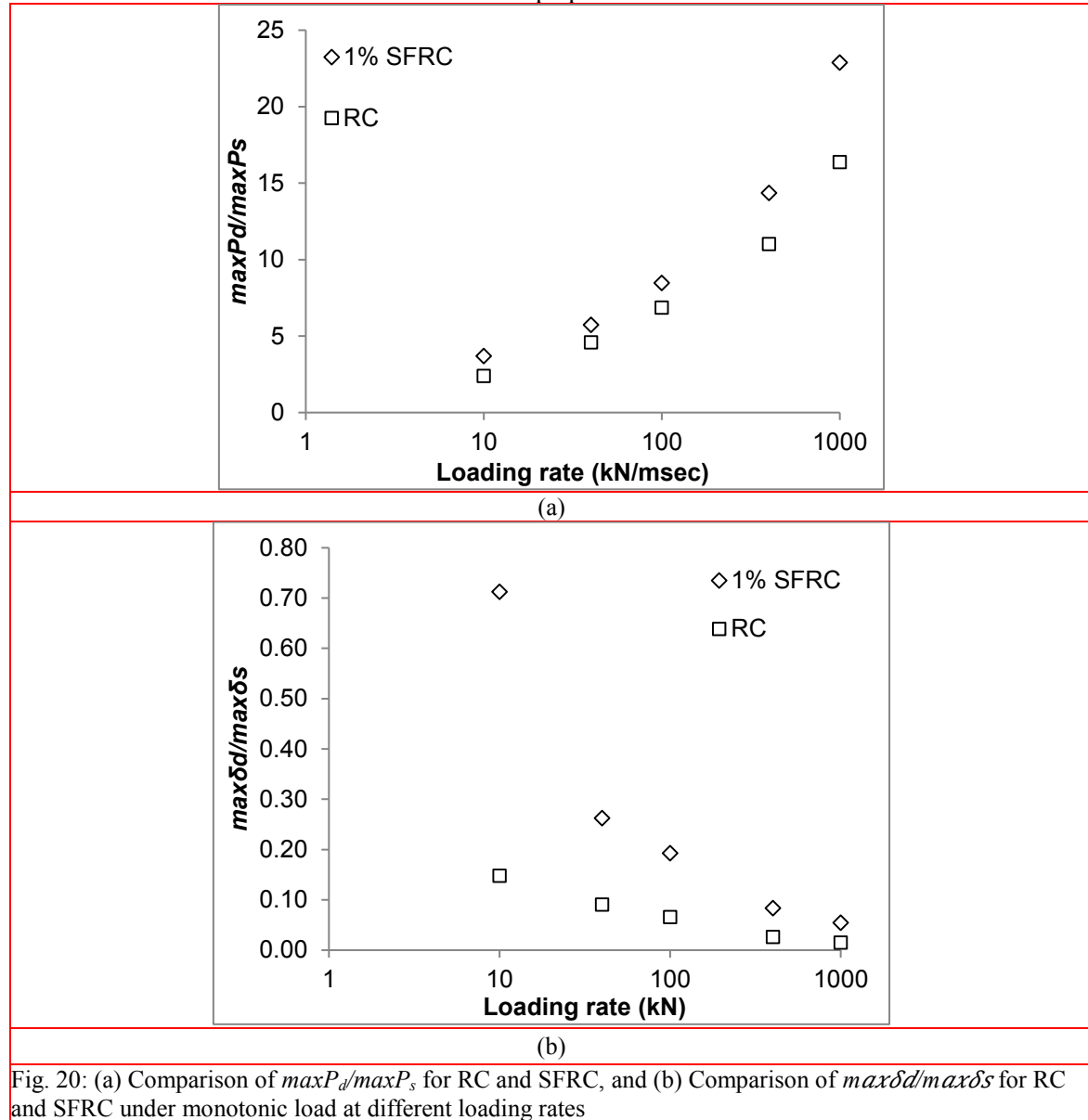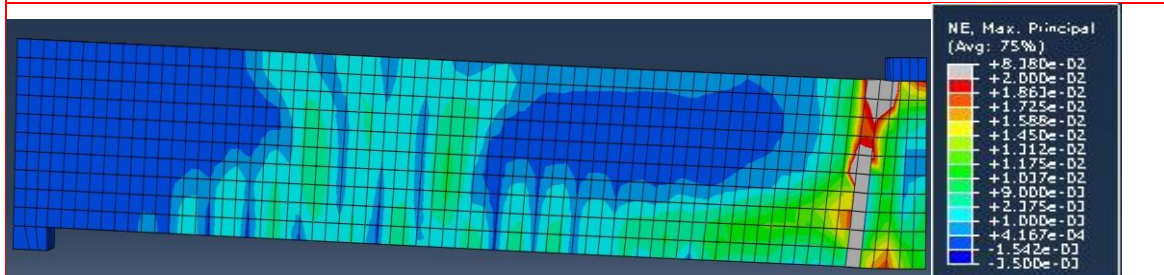
Fig. 21: (a) Comparison of $maxP_d/maxP_s$ for RC and SFRC, and (b) Comparison of $max\delta d/max\delta s$ for RC and SFRC under pulse load at different loading rates

(a)

(b)

(c)

(d)

(e)

Fig. 22: Principal strain distribution along the SFRC beam at maximum displacement (i.e. failure) for different pulse loading rates (a) 10kN/msec, (b) 40kN/msec, (c) 100kN/msec, (d) 400kN/msec, (e) 1000kN/msec
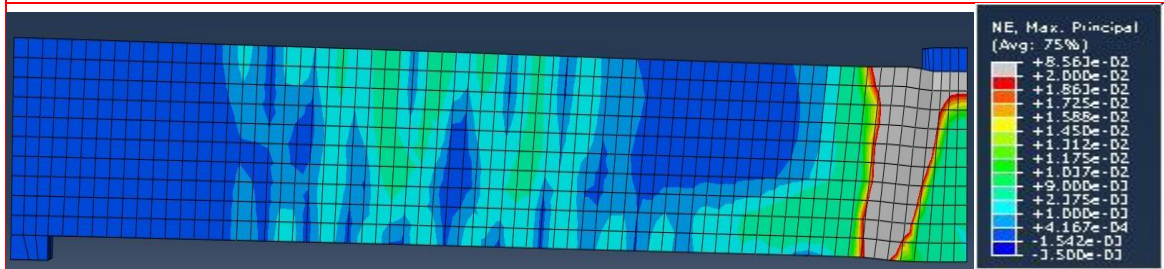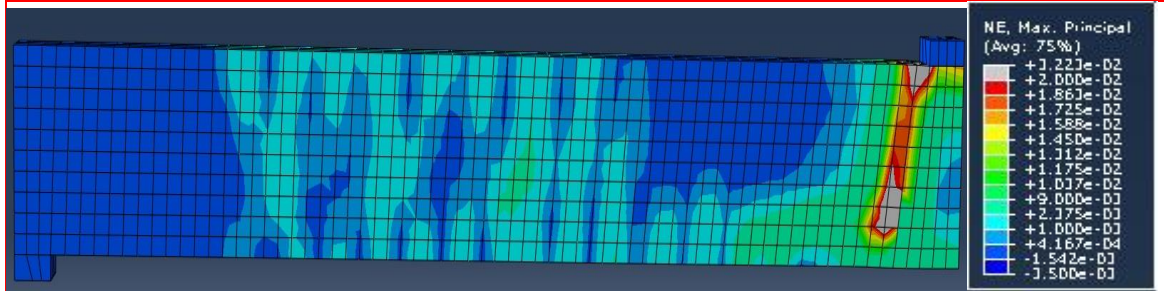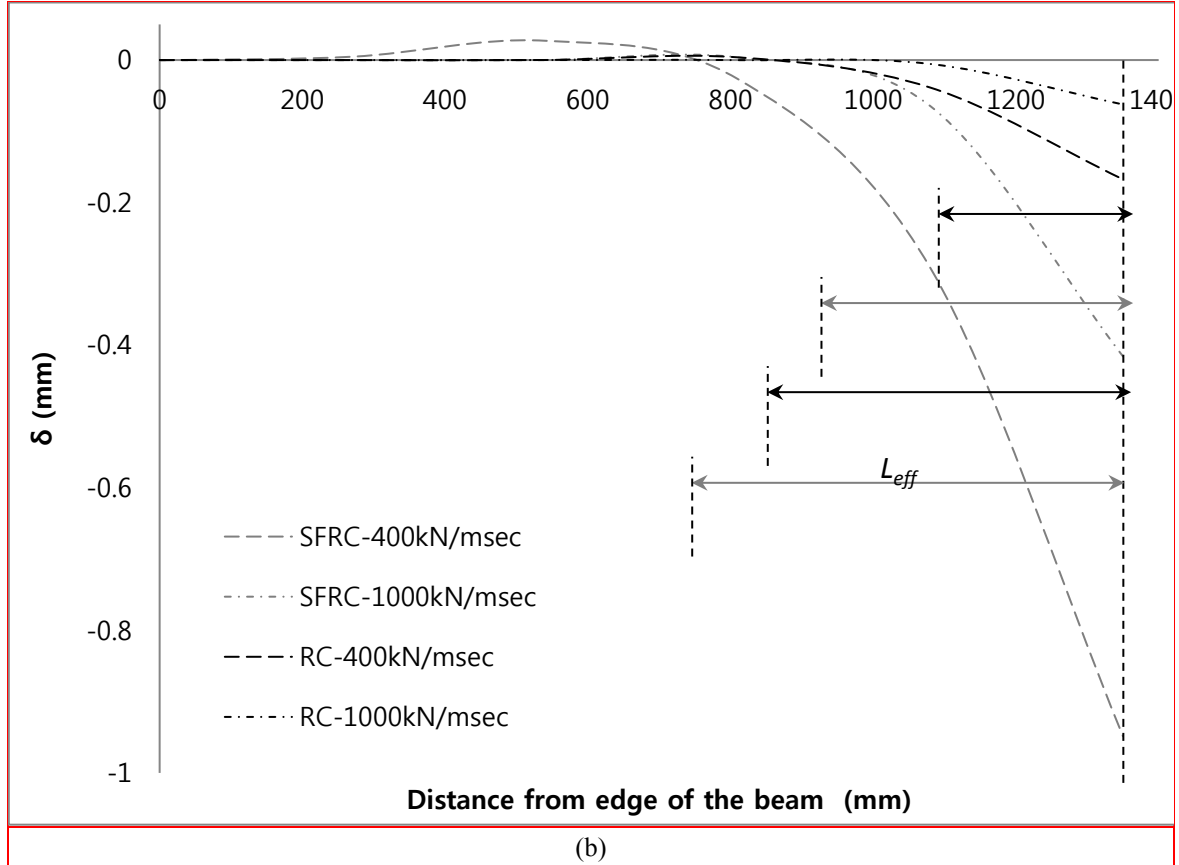
(a)

Fig. 23: Comparison between deflected shapes along RC and SFRC beams at the maximum contact force for pulse loading rate (a) 10, 40, 100kN/msec and (b) 400 and 1000kN/msec (the localized effective length L_{eff}, is also indicated)

8. Conclusions

A series of case studies were considered in order to investigate the structural responses of SFRC beams under static and impact loading conditions. Experimental work carried out as part of the present study on RC and SFRC beams with spans of 1.3 m is reported and has also been used to validate the subsequent numerical investigations (published test data on notched SFRC beams and full-scale beams were used as well). A simple, yet accurate and practical, brittle-cracking constitutive model for concrete was used by the NLFEA program adopted in the present study (i.e. ABAQUS) to analyse the behaviour of SFRC beams under impact loading applied at the mid span. For the beam cases considered, a comparative study between numerical and experimental data revealed that such constitutive models are capable of providing realistic predictions of the experimentally established behaviour of SFRC beams under increasing rates of loading. The results were also compared to numerical predictions using ABAQUS Damaged Plasticity model for concrete. The results show that the Brittle Cracking model, despite its simplicity, can provide accurate results (especially for cases where the response is dominated by tensile failure such as

beams under flexural loading and for brittle materials such as concrete). The key advantage is that the model has less variables to calibrate reducing the uncertainty usually associated with NLFEA predictions.

A comparison of the load-deflection curves under static and impact loads shows that under high-rate loading conditions, the response of both RC and SFRC beams becomes stiffer and allows the beam to attain higher levels of loading. This change in structural response is essentially linked to the deformation profile exhibited by the beams with increasing loading rates which becomes more localised and confined to the mid-span loading region (i.e. the area at which the load is exerted) as the loading rate increases. This is likely to be due to the influence of inertial forces of the localised *effective* part of the beam rather than due to changes in material properties, such as strain rate dependency. This due to the nature of stress waves invariably associated with impact, which reduces the length of the beam that responds to the applied load. This leads to an increase of the beam's stiffness and load-carrying capacity as well as to a reduction of its maximum vertical displacement under the load point as the loading rates increase. The study of RC and SFRC beam specimens shows that the use of fibres results in increase of load carrying capacity and energy absorption of the structural elements under impact. The deflection at the beam mid-span also increases compared to the RC case indicating the ductility provided by the steel fibres. The extent of the effective length around the point of application of the impact load seems to also improve due to the addition of fibres (albeit still decreasing as the loading rate increases).

The results also show the delay between the impact and reaction forces, which indicate that the fibres are slowing the rate at which the impact stress wave is travelling through the beam SFRC medium (similarly to experiments with the time delay reducing as the loading rate was increased, whilst the peak values of impact and reaction forces increase). Contours of principal strains were used to denote cracking patterns and the data shows the severity of the structural response as the loading rate is raised. The tensile strains at fibre pull-out were also highlighted, which shows that wider and deeper cracks are caused at higher loading rates. The presence of fibres seems to have expanded the region affected by the impact load. Crucially, it has allowed for the development of wider cracks that penetrate to the compression zone than in the case of static loading, indicating that the fibres have helped ensure the development of a more ductile flexural failure mode.

The NLFEA studies were also used to address a common shortcoming in impact experimental studies, which usually lead to the complete destruction of the specimen and often display *post*-failure characteristics of little value in terms of design. To address this, the impact loading was applied gradually in pulses in order to pin-point the *actual* failure point. This is useful in determining the load-carrying capacity of the beam, which is essential for impact-resistant design and assessment. A comparison between the pulse load and its monotonic counterpart reveals that the *true* load-bearing capacity of the RC and SFRC beams considered under impact loading is considerably lower than the values recorded experimentally. The study has also indicated the potential benefits for adding steel fibres, such as enhancements to strength, ductility, energy absorption and stiffness. This, along with the numerical tool developed and the potential for pin-pointing the actual load-carrying capacity, can form the basis of a practical impact-resistant assessment and design method for SFRC beams.

References

ABAQUS (2018), *Version 6.12-3 Documentation*, Available online at http://www.3ds.com/products-services/simulia/products/abaqus (accessed 03/09/2018).

Abbas, A.A., Pullen, A.D. and Cotsovos, D.M. (2010), "Structural response of RC wide beams under low-rate and impact loading", *Magazine of Concrete Research*, **62**, 723-740.

Abbas, A.A., Syed Mohsin, S.M. and Cotsovos, D.M. (2016), "A simplified finite element model for assessing steel fibre reinforced concrete structural performance", *Computers and Structures*, **173**, 31-49.

Abbas, A.A., Syed Mohsin, S.M., Cotsovos, D.M. and Ruiz-Teran, A.M. (2014), "Seismic response of steel fibre reinforced concrete beam-column joints", *Engineering Structures*, **59**, 261-283.

Abbas, A.A., Syed Mohsin, S.M., Cotsovos, D.M. and Ruiz-Teran, A.M. (2014), "Shear behaviour of SFRC simply-supported beams", *ICE Proc. Structures and Buildings*, **167**(SB9), 544-558.

Abbas, A.A., Syed Mohsin, S.M., Cotsovos, D.M. and Ruiz-Teran, A.M. (2014), "Nonlinear analysis of statically-indeterminate SFRC columns", *Structural Concrete*, **15**(1), 94-105.

Abbas, A.A., Syed Mohsin, S.M., Cotsovos, D.M. and Ruiz-Teran, A.M. (2014), "Statically-indeterminate SFRC columns under cyclic loads", *Advances in Structural Engineering*, **17**(10), 1403-1417.

Behinaein, P., Cotsovos, D.M. and Abbas, A.A. (2016), FE modelling of SFRC beams under impact loads, *ECCOMAS Congress 2016 VII European Congress on Computational Methods in Applied Sciences and Engineering*, M. Papadrakakis, V. Papadopoulos, G. Stefanou, V. Plevris (eds.), Crete Island, Greece, 5–10 June 2016.

British Standard Institution (2014), *Eurocode 2: Design of concrete structures — Part 1-1: General rules and rules for buildings.* BS EN 1992-1-1:2004+A1:2014 Incorporating corrigenda January 2008, November 2010 and January 2014.

British Standard Institution (2013), *Eurocode 8: Design of Structures for Earthquake Resistance — Part 1:* General rules, seismic actions and rules for buildings. BS EN 1998-1:2004+A1:2013 Incorporating corrigenda July 2009, January 2011 and March 2013.

Cotsovos, D.M. (2010), "A simplified approach for assessing the load-carrying capacity of reinforced concrete beams under concentrated load applied at high rates", *International Journal of Impact Engineering*, **37**(8), 907-917.

Cotsovos, D.M. and Pavlović, M.N. (2012), "Modelling of RC Beams under Impact Loading", *ICE Proceedings, Structures & Buildings,***165**, 2, 77-94.

Cotsovos, D.M., Stathopoulos, N.D. and Zeris, C. (2008), "Fundamental behaviour of RC beams subjected to high rates of concentrated loading", *ASCE Journal of Structural Engineering,* **134**, 1839-1851.

Destrée, X. (2001), "Steel fibre reinforcement for suspended slabs", *Concrete,* **35**(8),58-59.

Hughes, G. and Spiers, D.M. (1982), An Investigation on the Beam Impact Problem, *Cement and Concrete Association,* Technical Report 546.

Kishi, N. Khasraghy, S.G. and Kon-No, H. (2011), "Numerical simulation of reinforced concrete beams under consecutive impact loading", *ACI Structural Journal*, **108**(4), 444-452.

Kotsovos, M.D. (2015), *Finite-element Modelling of Structural Concrete: Short-term Static and Dynamic Loading Conditions,* Boca Raton, CRC Press.

Kotsovos, M.D. and Pavlović, M.N. (1995), *Structural concrete, Finite-element analysis for limit-state design,* Thomas Telford, London, UK.

Kotsovos, M.D., Pavlović, M.N. and Cotsovos, D.M. (2008), "Characteristic features of concrete behaviour: Implications for the development of an engineering finite-element tool", *Computers and Concrete*, **5**(3), 243-260.

Lok, T.S. and Xiao, J.R. (1999), "Flexural strength assessment of steel fibre reinforced concrete", *Journal of Materials in Civil engineering*, **11**(3), 188-196.

May, I.M., Chen, Y., Owen,D.R.J., Feng,Y.T. and Thiele, P.J. (2006), "Reinforced concrete beams under drop-weight impact loads", *Computers and Concrete*, **3**(2-3), 79-90.

Naaman, A.E. and Gopalaratnam,V.S. (1983), "Impact properties of steel fibre reinforced concrete in bending", *International journal of cement composites and lightweight concrete*, **5**(4), 225-233.

Nadine, M.P. (2011), "Healthy Doses of Steel Fibre 'Clear' Rebar Congestion in Concrete Coupling Beams", *ENR: Engineering News-Record,* **266**(2), 36.

RILEM Technical Committees (2003), "RILEM TC 162-TDF: Test and Design Methods for Steel Fibre-Reinforced Concrete, Final Recommendation: $\sigma - \varepsilon$ Design Method", RILEM *Materials and Structures*, **36**, 560-567.

Robins, P., Austin, S. and Jones, P. (2002), "Pull-out behaviour of hooked steel fibres", *Materials and structures*, **35**(7), 434-442.

Romualdi, J.P. and Batson, G.B. (1963), "Mechanics of crack arrest in concrete", *Journal of Engineering Mechanics*, **89**(EM3), 147-168.

Saatci, S. and Vecchio, F.J. (2009), "Nonlinear finite element modelling of reinforced concrete structures under impact loads", ACI *Structural Journal*, **106**(5), 717-725.

Trottier, J.F. and Banthia, N. (1994), "Toughness characterization of steel-fibre reinforced concrete", *Journal of materials in civil engineering*, **6**(2), 264-289.

Xu, Z., Hao, H. and Li, H.N. (2012), "Dynamic tensile behaviour of fibre reinforced concrete with spiral fibres", *Materials & Design*, **42**, 72-88.

Zhang, X.X., Abd Elazim, A.M., Ruiz, G. and Yu, R.C. (2014), "Fracture behaviour of steel fibre-reinforced concrete at a wide range of loading rates", *International Journal of Impact Engineering*, **71**, 89-96.

Zienkiewicz, O.C. and Taylor, R.L. (2013), *The Finite Element Method for Solid and Structural Mechanics, 7th Edition,* Butterworth-Heinemann, Oxford, UK.

Zisopoulos, P.M., Kotsovos, M.D. and Pavlović, M.N. (2000), "Deformational behaviour of concrete specimens in uniaxial compression under different boundary conditions", *Cement and concrete research*, **30**(1), 153-159.